Pre- to early-rift thermal conditions of the Upper Rhine Graben using geological and organic geochemical controls

Laurie Tchang-Tchong, Raymond Michels, Laurent Beccaletto, Claire Bossennec, Catherine Lorgeoux, Pierre Faure

Pre- to early-rift thermal conditions of the Upper Rhine Graben using geological and organic geochemical controls

Laurie Tchang-Tchong[1,2], Raymond Michels[1], Laurent Beccaletto[3], Claire Bossennec[4], Catherine Lorgeoux[1], Pierre Faure[2]

[1] Université de Lorraine, CNRS, GeoRessources, UMR 7359, France
[2] Université de Lorraine, CNRS, LIEC, UMR 7360, France
[3] BRGM, F-45060 Orléans, France
[4] Institute of Applied Geosciences, Geothermal Science and Technology, Technische Universität Darmstadt, Schnittspahnstraße 9, 64287 Darmstadt, Germany

Abstract

The Toarcian Posidonia Shale and Hettangian/Sinemurian Formation are the two main Mesozoic source rocks of the Upper Rhine Graben (URG). Their thermal maturities are measured and used to reconstruct the thermal history of the URG. However, the thermal maturity of these source rocks was impacted by: 1) the pre-rift burial history which includes a 120 My hiatus from Upper Jurassic to the Paleocene; 2) the syn- and post-rift burial histories; and 3) the current high geothermal gradients and associated hydrothermal convective cells. In this study, the Saverne Fracture Field is considered the pre-rift analogue of the URG and therefore bears witness to the pre-rift thermal history. It was isolated from the graben upon its opening, i.e. in the Priabonian, and contains the same Mesozoic rocks, which, in contrast to the URG, are currently outcropping. As the source rocks in the Saverne Fracture Field were not buried as in the URG, their thermal maturities should be a consequence of the Upper Jurassic/Cretaceous burial only. Organic geochemistry results indicate that they are of pre-oil window thermal maturity. Calibration of the Saverne Fracture Field thermal model for the pre-rift period of the URG allows us to estimate that during the Upper Jurassic/Cretaceous hiatus additional burial did not exceed about 300 m. The additional sediments cannot be attributed specifically to the Upper Jurassic or Cretaceous. However, simulation results indicate that if Cretaceous sediments were deposited, they had to be preserved until the Paleocene, and their maximum cumulative thickness must have been at most 100 m. In addition, thermal modelling indicates that during the very first onset of the URG, Mesozoic sediments could have been buried again by about 250 m of Cenozoic sediments, with negligible effect of the pre-rift thermal signature. These geochemical and geological constraints are key input for further URG thermal modelling. Indeed, such constraints on the pre-rift thermal history should allow future assessment of the syn-rift burial and recent hydrothermal convective cells impact on the Mesozoic source rocks maturity.

Keywords

Upper Rhine Graben, basin thermal modelling, paleoburial, pre-rift, Cretaceous hiatus, Toarcian Posidonia Shale, homohopanes, steranes

1 Introduction

The Upper Rhine Graben (URG) is a Cenozoic intracontinental rift with significant local thermal anomalies. Historically, it was the focus for research on hydrocarbon resources and more recently on deep geothermal energy (e.g., Frey et al., 2022a, 2022b). This is precisely the case for the Pechelbronn sub-basin, located in the western central part of the URG, which was mentioned as early as the end of the 15th century for its hydrocarbon resources (Schwarz, 2021) and hosts a geothermal field studied since the end of the 19th century (Gérard and Kappelmeyer, 1987). Deep geothermal energy is a key renewable energy (e.g., Frey et al., 2022) that raises other strategic challenges, such as the extraction of lithium from geothermal brines (e.g., Fries et al., 2022; Sanjuan et al., 2022). As a result, understanding and evaluating the diagenesis, porosity and permeability properties of geothermal reservoirs is of major importance. The evolution of these properties is controlled by burial and the thermal history of the basin (Schmoker and Gautier, 1988; Schmoker and Hester, 1989; Kupecz et al., 1997). In addition, the same control factors are involved in evaluating petroleum systems, which depend on burial, time and temperature (e.g., Philippi, 1965; Welte, 1966; Bajor et al., 1969). Consequently, because the URG is one of the main targets of geothermal projects in Central Europe (Frey et al., 2022a), it is essential to reconstruct the evolution of its burial and thermal history. Generally, thermal maturity assessment of organic matter allows calibration of the burial and thermal reconstructions. As the primary source rocks of the URG are of Liassic age (Böcker and Littke, 2016, and references therein), they experienced the burial history of the eastern Paris Basin prior to that of the URG (i.e., prior to the Priabonian). Their maturities can be at least attributed to three superimposed unknowns of burial and thermal conditions: 1) the sedimentation hiatus of more than 120 My from the Upper Jurassic to the Paleocene (Schnaebele, 1948; Ziegler, 1990; Ménillet et al., 2015); 2) the syn- and post-rift burial histories (Schumacher, 2002; Buchmann and Connolly, 2007; and the references therein); and 3) the current high geothermal gradients and associated hydrothermal convective cells (e.g., Kohl et al., 2000; Baillieux et al., 2013). Thus, to reconstruct the full burial and thermal history of the basin, the part related to the Upper Jurassic/Paleocene hiatus must be resolved first.

The Saverne Fracture Field is adjacent to the Pechelbronn sub-basin and is part of the current western margin of the URG (**Figure 1**; Genre, 1981; Sissingh, 2006). The Saverne Fracture Field has been isolated from the URG since its opening (Ménillet et al., 1979, 2015; Genre, 1981) and Liassic source rocks are preserved as outcrops today (Chantraine et al., 1996). Their thermal maturities acquired during the Upper Jurassic to Paleocene (represented today by a stratigraphic hiatus) have not been affected by the syn- and post-rift burial histories and the current high geothermal gradients and associated hydrothermal convective cells. The Saverne Fracture Field thus provides the opportunity to evaluate the maximum burial depth reached by the Mesozoic pre-rift sediments during Upper Jurassic/Cretaceous times, prior to the onset of the URG rifting.

In this study, the thermal maturity data measured on outcropping Mesozoic rock samples from the Saverne Fracture Field are used to calibrate thermal basin models to estimate the maximum burial depth reached before the development of the URG *sensu stricto*, i.e. before the Priabonian. By analogy, this provides geological and geochemical conditions of the URG pre-rift thermal history. The work proposes burial models based on: 1) a bibliographical synthesis of the tectono-sedimentary history of the URG, in particular its pre-rift period; 2) the characterization and assessment of the thermal maturity of the organic matter contained in Mesozoic rocks; and 3) the integration of the results into the PetroMod© Software to calibrate the URG pre-rift thermal history, by adjusting the paleoburial.

2 Geological background of the URG

2.1 General geological features of the URG

The URG belongs to the European Cenozoic Rift System (ECRIS), a 1100 km long rift system initiated in the Eocene and extending from the North Sea to the Western Mediterranean (Dèzes *et al.,* 2004). The NNE/SSW trending URG extends over 300 km from the Rhenish Massif to the north to the Jura Mountains and its current geometry corresponds to a set of asymmetrical and antithetical half-grabens, connected by transfer zones inherited from Paleozoic basement structures (Schumacher, 2002; Derer, 2003; Roussé, 2006; Hinsken et al., 2007; Grimmer et al., 2017). It is limited to the west by the Vosges Mountains, the eastern Paris Basin and the Saverne Fracture Field, and to the east by the corresponding units of the Black Forest, Odenwald and Franconian Platform. The present-day URG is limited by the Western and Eastern Main Border Faults. Its opening and development were controlled by the Pyrenean and Alpine orogen dynamics (Schumacher, 2002; Dèzes *et al.,* 2004), resulting in a polyphase tectonic rift evolution and related syn- to post-rift sedimentation (Laubscher, 1987; Sissingh, 1998, 2006; Schumacher, 2002).

2.2 The Saverne Fracture Field

This study focuses on the western central part of the URG, corresponding to the Saverne Fracture Field and the easterly adjacent Pechelbronn sub-basin whithin the Haguenau block as defined by the GeORG project (**Figure 1**c; Équipe du projet GeORG, 2013). The Saverne Fracture Field is a crescent-shaped 90 km long and up to 20 km wide highly-faulted structure located between the URG and the eastern Paris Basin (**Figure 1**b and c). The Paris Basin and the Franconian Platform are intracratonic basin systems, where up to 2 to 3 km of sediments accumulated during Triassic and Jurassic (Ziegler and Dèzes, 2005, and references therein). The sedimentary deposits in these basins were eroded to the Lower Triassic (Buntsandstein), while preserved in the Saverne Fracture Field which contains both pre-rift sediments from Lower Triassic to Bajocian formations and Middle Eocene early-rift sediments (**Figure 1**b and c; Ménillet et al., 1979, 2015; Chantraine et al., 1996).

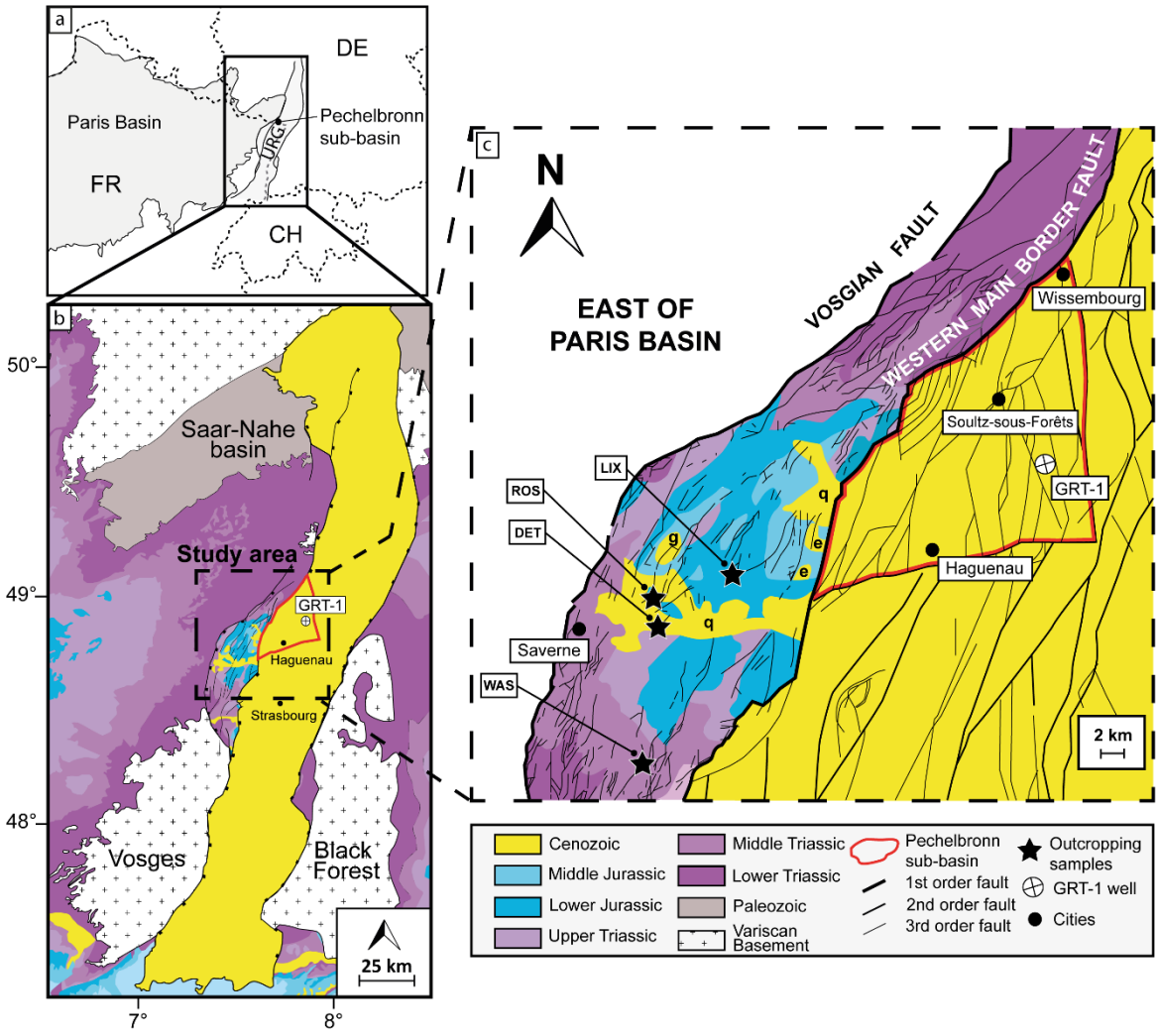

Figure 1 Location of studied area. *a. Simplified map of the borders between France, Germany, Switzerland with east Paris Basin, the URG and location of the Pechelbronn sub-basin. b. Simplified geological map of the URG surroundings with limits of the study area and Pechelbronn sub-basin. Location of the geothermal GRT-1 well (crossed circle). c. Zoom on the study area represented by a schematic structural map with the outcropping formations of the Saverne Fracture Field. Black stars: sampling locations. q: Plio-Quaternary; g: Oligocene; e: Eocene; LIX: Lixhausen quarry; ROS: Rosenwiller; DET: Dettwiller; WAS: Wasselonne quarry.*
Based on Équipe du projet GeORG (2013) and the geological map of France 1/1 000 000, BRGM.

2.3 Pre-rift and early-rift tectono-sedimentary history of the URG and the surrounding areas

The oldest rocks in the area are known in the Vosges, the Black Forest and Odenwald massifs and are related to the pre- and syn-Variscan orogeny (Edel and Fluck, 1989; Lardeaux et al., 2014). During the latest Carboniferous-early Permian, the area of the future URG, the Saverne Fracture Field, the eastern Paris Basin and the Franconian Platform experienced disruption and collapse of the Variscan orogen (Schumacher, 2002; Ziegler and Dèzes, 2005). Uppermost Carboniferous to Lower Permian continental clastics were deposited in vast fault-controlled basins, such as the Lorraine-Saar-Nahe and the Kraichgau basins, known either at outcrops or identified beneath the Mesozoic cover of the Paris and Germanic basins (Boigk and Schöneich, 1970; Donsimoni, 1981; Scheck-Wenderoth et al., 2008).

From the Late Permian until at least the mid-Jurassic, this area underwent post-orogenic thermal subsidence (Cloethingh and Ziegler, 2007). This tectonic regime led to the formation of the Paris Basin and Franconian Platform, both belonging to the same epicontinental paleogeographic domain, namely the southern part of the Central Europe Basin System located north of the passive northern margin of the Alpine Tethys (Ziegler, 1990; Geyer et al., 1991; Bourquin et al., 2006; Scheck-Wenderoth et al., 2008). The area experienced a limited geological evolution, only determined by eustatic sea-level changes, low-grade regional subsidence and diffuse crustal stretching (Ziegler and Dèzes, 2005; Scheck-Wenderoth et al., 2008).

The first Mesozoic deposits are represented mainly by the fluvial Buntsandstein sandstones (Bourquin and Guillocheau, 1996; Bourquin et al., 2006, 2009), grading into Middle Triassic claystones, limestones and dolostones (Muschelkalk facies) (**Figure 2**; Ziegler, 1990; Ménillet et al., 2015). In the Late Triassic, the sedimentation evolved to evaporitic deposits (Keuper facies) due to marine regression from the Germanic Basin (Bourquin and Guillocheau, 1996; Bourquin et al., 2002). The Tethysian transgression at the Early Jurassic led to the deposition of carbonates and shales during Hettangian-Sinemurian, followed by thick shales from Pliensbachian to Aalenian (**Figure 2**; Schnaebele, 1948; Schirardin, 1960; Megnien, 1980). These Liassic deposits contain the main source rocks of the URG, also extending over the entire Central Europe Basin System (Littke et al., 2008). These formations were followed by Dogger carbonates until the Callovian-Oxfordian transgression, which was marked by marl deposits (Wetzel et al., 2003; Blaise et al., 2011; Landrein et al., 2013). The end of Jurassic is characterized by carbonate platform deposits of Upper Oxfordian, Kimmeridgian and Tithonian (Curnelle et Dubois, 1986; Landrein et al., 2013).

The eastern Paris Basin, the Saverne Fracture Field, the URG and the Franconian Platform do not show evidence of Cretaceous sedimentation (**Figure 1**). The absence of Cretaceous deposits may result from a combination of a low eustatic sea level during the Early Cretaceous (Scheck-Wenderoth et al., 2008) and the uplift of the “Rhenish Shield” (Cloos, 1939; Illies, 1975; Duringer, 1988; Geyer et al., 1991; Ziegler, 1994; Walter, 1995; Schumacher, 2002; Le Roux and Harmand, 2003; Timar-Geng et al., 2006; Bourgeois et al., 2007; Scheck-Wenderoth et al., 2008). The large uplifted domain involves notably the future URG (Schumacher, 2002) and the Saverne Fracture Field areas, which were then affected by the intraplate so-called “Laramide” compression during the late Cretaceous/Paleocene (Ziegler, 1987). This slight compressional phase led to moderate folding and southward tilting of the Mesozoic series in the whole area, triggering their erosion before syn-rift sedimentation (Sittler, 1967; Ziegler, 1990; Lutz and Cleintuar, 1999; Bourgeois et al., 2007; Grimmer et al., 2017). Indeed, in contrast to the central and western Paris Basin, most of the Malm and all of the Cretaceous deposits are not found in the URG beneath the syn-rift deposits (the youngest pre-rift sediments are Oxfordian-Kimmeridgian) (Wannesson, 1998).

The early-rift phase started in Middle Eocene (Lutetian) and is evidenced by volcanic activity (Schumacher, 2002; Lutz et al., 2013), e.g. the Basalte de Gundershoffen Formation

in the study area (Ménillet et al., 2015; and references therein). The first Cenozoic sediments correspond to siderolitic formations and residual clays resulting from weathering of the Mesozoic carbonates (Sittler, 1965; Duringer, 1988; Schumacher, 2002; Duringer *et al.,* 2019). These weathering products are locally associated with lignite-rich Lutetian lacustrine sediments, e.g. the Bouxwiller Formation in the Saverne Fracture Field and the URG (**Figure 1** and **Figure 2**; Sittler, 1965; Ménillet et al., 2015; and references therein). This slight resumption of subsidence marks the early rifting phase and is characterized by the deposition of marly clays and calcareous formations of Bartonian age (Châteauneuf and Ménillet, 2014; Duringer et al., 2019). These sediments are sparsely recorded in the Saverne Fracture Field (Châteauneuf and Ménillet, 2014) and certainly correspond to the last sediments deposited before its isolation from the URG (Ménillet et al., 1979, 2015; Genre, 1981). The onset of the rifting was initiated following this period, probably at Priabonian (Duringer, 1988; Berger et al., 2005; Derer et al., 2005; Ménillet et al., 2015). During the early Oligocene, the URG was episodically flooded by marine ingressions, as reflected by the deposition of fossil-rich marine marls, referred as the Middle Pechelbronn layers in its central part (Martini and Reichenbacher, 2007). The Pechelbronn Gp. of Rupelian age (Early Oligocene) is made of siliciclastic and evaporitic rocks representing the syn-rift stage. The transition to the post-rift stage is then marked by the deposition of the Marnes à Foraminifères Formation at the base of the Série Grise (**Figure 2**), whose uniform facies and thickness throughout the URG testify to a general flooding from middle to late Rupelian (Oligocene) (Schumacher, 2002).

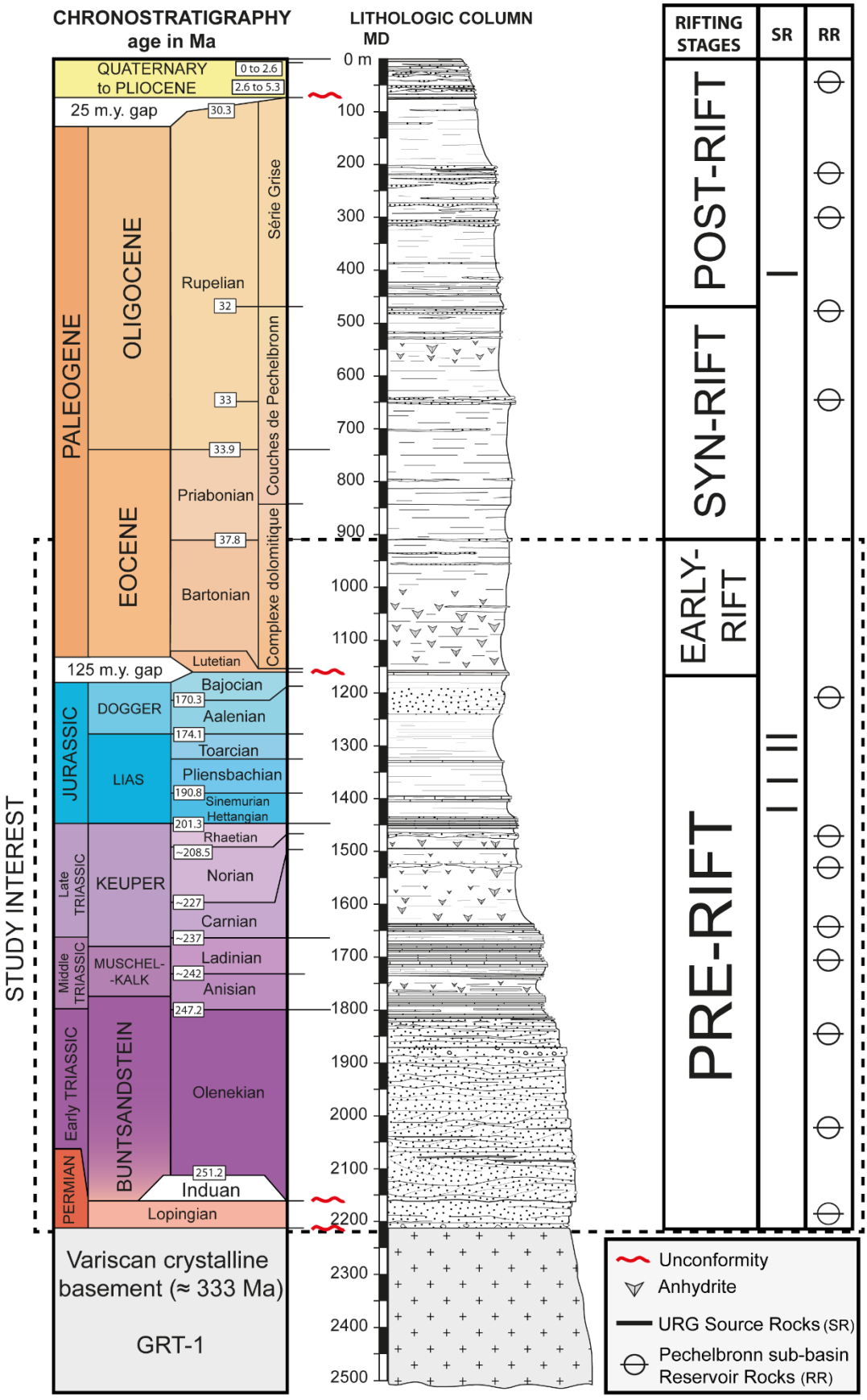

Figure 2 Chrono-lithostratigraphic log of GRT-1 well modified after Duringer et al. (2019) with the period of interest framed in black dotted lines. *The main source rocks of the central URG (SR) are identified according to Wannesson (1998), Böcker et al. (2016), and references therein. Main reservoirs (RR) of the Pechelbronn sub-basin are represented according to Schnaebele (1948), Wannesson (1998) and Bossennec (2019).*

3 Sampling and analytical procedures

Nineteen fresh outcrop rock samples collected along the Paris-Strasbourg high-speed train worksites (Toarcian, Pliensbachian, Hettangian/Sinemurian, Late and Middle Triassic – respectively Keuper and Muschelkalk facies - ages) and two quarries (Pliensbachian, Hettangian/Sinemurian and Middle Triassic - Muschelkalk facies - ages) in the Saverne Fracture Field (Figure 1c) were selected. The facies and stratigraphic level of the samples are presented in **Table 1**.

The rock samples were crushed, sieved (<180 µm mesh) and analyzed by Rock-Eval pyrolysis at the Institut des Sciences de la Terre d'Orléans (ISTO) laboratory (France) (**Table 1**; analytical procedure described in Le Meur et al., 2021). Powered rock samples (20-30 g) were also extracted with dichloromethane (DCM) using an Accelerated Solvent Extractor (ASE 350, Dionex) at 100 bar and 130°C (Li et al., 2002; Hautevelle et al., 2006; Biache et al., 2015). The organic extracts were dried, weighed and taken up in hexane for the SARA fractionation method (analytical procedure described in Abuhelou et al., 2017). Using the automated ASPEC GX-274 (Gilson), fractionation was carried out using Strata CN cartridges (500 mg, 3 mL, Phenomenex) to which 1 g of activated silica was added. The aliphatic fractions were analyzed for biomarkers using an Agilent Technologies 8890 GC equipped with a silica DB5-MS column (60 m × 0.25 mm id × 0.25 µm film thickness) coupled to an Agilent Technologies Triple Quadrupole 7000/7010 MS operating in alternated full scan/single-ion monitoring (SIM) mode. The oven temperature was programmed as follows: 70 °C (held 2 min) to 130 °C at 15 °C/min, then 130 to 315 °C at 4 °C/min, and then 325 °C (held 25 min). The carrier gas was helium at 1.4 mL/min constant flow. The injection was set in splitless mode at 300 °C. Biomarkers were identified using GC-MS/MS and according to the literature.

Sample	Locality	Stratigraphic formation	Facies	Stage/ Age	Rock-Eval pyrolysis data						Biomarkers ratios				
					TOC (%)	Tmax (°C)	S1 (mg HC/ g rock)	S2 (mg HC/ g rock)	HI (mg HC/ g TOC)	OI (mg HC/ g TOC)	RC_{30} (%)	RC_{31} (%)	RC_{32} (%)	RC_{29} (%)	R^*C_{29} (%)
2T4	ROS.	Couches à *Dactylioceras c.*	Laminated marl, clay-rich facies	Toarcian	3.39	432	0.02	15.96	471	13	31	22	18	14	29
2T3	id.	Schistes carton	id.	id.	3.21	432	0.02	16.31	508	15	30	22	17	8	24
2T2	id.	id.	Laminated marl, carbonate facies	id.	0.96	423	0.02	5.03	524	43	20	29	25	15	26
2T1	id.	id.	Laminated marl, organic-rich facies	id.	8.03	424	0.19	58.85	733	15	22	27	26	10	23
2P7	id.	Calcaire de Kirrwiller	Marls	Pliensbachian	0.66	439	0.01	0.66	100	11	46	24	14	14	27
2P5	id.	Marnes à *Septaria*	id.	id.	0.75	437	0.01	0.66	88	15	45	25	15	16	24
2P4	id.	id.	id.	id.	0.89	438	0.01	0.84	94	28	46	25	15	17	24
2P3	id.	id.	id.	id.	0.95	439	0.06	1.19	125	8	43	28	18	18	19
2P2	id.	id.	id.	id.	1.03	441	0.01	1.18	115	10	45	25	15	14	23
2P1	id.	id.	id.	id.	0.93	440	0.01	0.97	104	11	44	26	16	12	20
2P18	LIX.	Marnes à Ovoïdes	id.	id.	0.71	436	0.01	0.71	100	14	41	37	21	24	21
2P13	id.	id.	id.	id.	0.73	436	0.01	0.7	96	5	41	37	22	21	20
2P8	id.	id.	id.	id.	0.74	437	0.02	0.82	111	14	40	36	22	20	22
2H	DET.	Calcaires et marnes à Gryphées	id.	Hett./Sine.	2.9	422	0.21	14.65	505	22	23	44	35	22	28
2H2L	LIX.	id.	id.	Hett./Sine.	2.06	424	0.05	11.54	561	51	20	48	46	24	26
2R1	DET.	Argiles de Levallois	Oxidized siltstone	Rhetian	0.15	405	0.02	0.1	67	127	40	57	49	26	17
2R2	id.	Grès Rhétiens	Clayey siltstone	id.	0.81	431	0.01	0.53	65	4	41	59	56	28	31
2K	id.	Marnes Irisées Supérieures	Marls	Late Triassic	-	-	-	-	-	-	14	57	61	24	45
2M	WAS.	Couches à Cératites	Limestone	Middle Triassic	0.17	440	0.01	0.42	245	116	20	60	58	45	43

Table 1 Rock-Eval pyrolysis and molecular geochemistry results measured on outcrop samples from the Saverne Fracture Field. *Locality abbreviations: ROS: Rosenwiller; LIX: Lixhausen quarry; DET: Dettwiller; WAS: Wasselonne quarry. Rock-Eval pyrolysis parameters and biomarkers ratios abbreviations: HI: Hydrogen Index; OI: Oxygen Index; Biomarkers maturity parameters (Peters et al, 2005a, 2005b): RC_{30} (%): βα/(βα+αβ) C_{30} hopane; RC_{31} (%): 22S/(22S+22R) C_{31} homohopane; RC_{32} (%): 22S/(22S+22R) C_{32} homohopane; RC_{29} (%): 20S/(20S+20R) C_{29} 5α(H),14α(H),17α(H) steranes; R^*C_{29} (%): ββ/(ββ+αα) C_{29} steranes.*

4 Modelling procedures

4.1 Synthetic lithostratigraphy column based on the GRT-1 geothermal well

The 1D thermal modelling was performed using the PetroMod© software, version 2022.1. Numerical and maturity modelling concepts were previously published by Waples et al., (1992b, 1992a), Yalcin et al. (1997), and Poelchau et al. (1997). The primary inputs are listed in **Table 2** and **Table 3**. The stratigraphic formations were based on the description of the geothermal well GRT-1 from (**Figure 2**; Duringer et al., 2019). Stratigraphic ages were derived from the same publication and based on the international chrono-stratigraphic chart revised in 2019 (Cohen et al., 2013). The lithological mixes were derived from the explanatory note of the Haguenau geological map (Ménillet et al., 2015). The stratigraphic formations thicknesses are based on the measured depth (Duringer et al., 2019) as corrected for the slight well deviation (Baujard et al., 2017), providing the true vertical depth (Genter, personal communication). As visible in the GRT-1 well, the Bajocian was partially eroded to approximately 30 m of preserved rock. As deduced from Landrein et al. (2013), the thickness eroded was evaluated to 50 m and added into the burial model (bringing the total initial thickness to 80 m). Moreover, as the Bathonian and the Callovian units were deposited across the whole Jurassic carbonate platform, these formations were added to the synthetic stratigraphic column (**Table 2**), i.e. 50 m and 60 m, respectively (Böcker, 2015).

For all model strategies, organic thermal maturity markers were used to calibrate the thermal history (Burrus, 1986; Makhous and Galushkin, 2004; Hantschel and Kauerauf, 2009), considering fixed time-temperature couples. This assumption was made possible as time is determined from the lithostratigraphic description (Cohen et al., 2013; Duringer et al., 2019) and temperature from the boundary conditions (see subsection 4.2). Input data were adjusted to fit the simulated and measured maturity markers values by adding or removing sediment thickness of Upper Jurassic and presumed Cretaceous age. After estimating the maximum thickness of sediments, modelling was conducted considering the onset of the URG at the late Eocene. Lutetian and Bartonian layers were added to the model after consideration of the associated Eocene thermal peak (**Table 3**).

4.2 Boundary conditions

To calculate the temperature gradient and resulting paleo-heat flow within a basin, model boundary conditions (heat convection, heat conduction and radiogenic heat production) have to be defined (Bruns et al., 2016). The software systematically calculated the radiogenic heat production in the sedimentary column according to the lithological mix. The sediment-water interface temperature (SWIT, in °C) and the paleo-water depth (PWD, in m) were used to estimate the temperature at the top of the sedimentary column through time. Finally, the evolution of the basal heat flow over time is based on Bossennec et al. (2021; see below).

In this study, the PWD data from the Permian to the Upper Jurassic (145 Ma) were derived from Blaise (2012). Its evolution varies between 0 m and 100 m accordingly to paleo-environments, e.g., 100 m corresponding to the Liassic clay-rich facies. PWD values were considered as 0 m, from the end of the Jurassic to the Paleocene, followed by the deposition of exclusively continental paleo-environments during Middle Eocene (Ménillet et al., 2015; Duringer et al., 2019). The SWIT was determined according to Bruss (2000), who compiled temperature data based on palynological and palynofacies studies of the URG from Stahmer (1980), Schuler (1990) and Sittler and Ollivier-Pierre (1994). Finally heat flow from Bossennec et al., (2021) were used. These authors estimated its value by calibrating the temperature derived from $\delta^{18}O$ measured in quartz overgrowths of URG Buntsandstein samples with burial temperature profiles modelled under OpenFlow© and based on Böcker (2015). For the pre-rift period, the following scenario was used: Heat flow of 65 mW/m² at the beginning of the

Permian, progressively increasing to 80 mW/m² at 180 Ma, decreasing to 73-72 mW/m² at the end of the Jurassic, and an almost constant value (≈ 70 mW/m²) until 90 Ma. With the URG opening, the heat flow increased to 100 mW/m² during the Paleocene from 60 to 50 Ma, and remained constant until the Priabonian.

4.3 Biomarker kinetic parameters

Organic matter (OM) deposited in sedimentary basins is transformed during geological history in response to burial, temperature and time (Philippi, 1965; Welte, 1966; Bajor et al., 1969). Constituents of the transformed OM, e.g. the biomarkers, record information about the thermal history of sedimentary basins. Biomarker reactions depend on time and temperature and are therefore characterized by their kinetic parameters (Seifert and Moldowan, 1980; Mackenzie and McKenzie, 1983; Gallagher and Evans, 1991; Marzi, 1992; Landais and Elie, 1999).

In this study, the kinetic parameters for the isomerization of hopanes at C_{22} (activation energy: 0.016 s^{-1}; pre-exponential factor: 91 kJ mol^{-1}) and steranes at C_{20} (activation energy: $6*10^{-3}$ s^{-1}; pre-exponential factor: 91 kJ mol^{-1}) from Mackenzie and McKenzie (1983) were used for calibration. Modelling was performed using the C_{31}-homohopanes and C_{29}-steranes S/(S+R) isomerization ratios.

4.4 Thermal simulations strategies

As conducted using PetroMod© software, burial and thermal modelling consisted of comparing the evolution of the C_{31}-homohopanes and C_{29}-steranes S/(S+R) isomerization ratios determined on the sample set (**Figure 6**) with simulated values as a function of depth. For the basin modelling of pre-rift and early-rift periods, a synthetic reference stratigraphic column was constructed (**Table 2**) between the top of the basement at 259.8 Ma to the Marnes et Calcaires d'Ettendorf Formation at 170 Ma (layer 47 Bajocian, in **Table 2**). A short Induan age hiatus follows the Permian deposits, then from the Grès Vosgien Gp. (250 Ma) to the Toarcian, the domain was gradually buried by thermal subsidence. After the Cimmerian tectonic phase (Toarcian-Aalenian limit) (Robin, 1995; Guillocheau et al., 2000), the Marnes et Calcaires d'Ettendorf Formation was deposited, indicating the development of carbonate platforms.

The first strategy (strategy No.1, **Table 4**) aimed to evaluate the maximum thickness of sediment deposited during the hiatus. Böcker (2015) speculated 400 m of Malm in his thermal model. Based on the literal interpretation of the literature, five simulations considered the deposition of 0 m, 100 m, 200 m, 300 m or 400 m of Malm followed by a hiatus period from 140 to 70 Ma. The simulation ended with the partial erosion of Bajocian and the complete erosion of Bathonian, Callovian and Malm during the Paleocene (from 60 to 50 Ma) (**Figure 6**a and b).

The second strategy (strategy No.2, **Table 4**) aimed to assign the estimated sediment thickness to a stratigraphic age, i.e. to the Jurassic or Cretaceous. In this perspective, a first simulation considered gradual sediment deposition from 160 to 70 Ma with 200 m of Malm and 100 m of continental to coastal facies sediments of Cretaceous age, followed by the partial erosion of Bajocian and the complete erosion (from 60 to 50 Ma) of Cretaceous, Malm, Callovian and Bathonian (red curve on **Figure 6**c and d). The second simulation considered the deposition of 300 m of Malm (from 160 to 145 Ma) followed by a hiatus period from 140 to 70 Ma, which ended with the partial erosion of Bajocian and the complete erosion of Malm, Callovian and Bathonian from 60 to 50 Ma (black curve on **Figure 6**c and d). The third simulation considered the deposition of 200 m of Malm followed by alternations of deposition and erosion episodes during Cretaceous. Maximum cumulative thickness considered was 100

m (as to have an expected impact on biomarkers thermal maturity) before start of erosion at 60 Ma (green curve on **Figure 6**c and d).

The third strategy (strategy No.3, **Table 4**) considered the early-rift period (**Table 3**) as a sensitivity test on the simplest simulated pre-rift model (black curve on **Figure 6**c and d). This strategy considered the presence of Eocene deposits in the Saverne Fracture Field (**Figure 1**c) and its isolation from the URG at the beginning of Priabonian (**Figure 7**). This was tested with regard to the thickness of 253 m of Lutetian and Bartonian deposits from the GRT-1 well (**Figure 2**; Duringer et al., 2019).

	PRE-RIFT MODEL						
	Stratigraphic formation	Modelled layer name	Age (Ma)	Thickness (m)	Eroded thickness (m)	Event type	Lithological Mix (%)
	-	63 Selandian	60	0	-(?) m	E	-
	-	62 Maastrichtian	to 70	0	(?)	H	-
	-	55 Berriasian	from 140				-
	-	54 Tithonian	145.1	0	(?)	D	-
	-	53 Tithonian	150	0	(?)	D	-
	-	52 Kimmeridgian	155	0	(?)	D	-
	-	51 Oxfordian	160	0	(?)	D	(?)
	Not differentiated	50 Callovian	165	0	60	D	Ml(50),Sh(20),Si(10),Sh(10),Ss(10)
	Not differentiated	49 Bathonian	167	0	50	D	Ml(35),Sh(25),Si(15),Li(10),Ss(10),Sh(5)
	Grande Oolithe	48 Bajocian	169	0	50	D	shLi(72),Sh(26),PY(2)
SYNTHETIC REFERENCE STRATIGRAPHIC COLUMN	Marnes et Calcaires d'Ettendorf	47 Bajocian	170	32	-	D	Li(90),Ml(10)
	Argiles Sableuses	46 Aalenian	171	4	-	D	Sh(85),Ss(15)
	Formation de Schalkendorf	45 Aalenian	172	39	-	D	Si(50),Ss(22),Sh(8),Li(8),Ml(8),PY(6)
	Formation de Gundershoffen	44 Aalenian	174	39	-	D	Sh(45),Si(15),Li(15),Ss(12),PY(5),GY,KAO,IL&CH(3 ea.)
	Formation de Printzheim	43 Aalenian	175	32	-	D	Ml(60),Si(25),bSh(10),PY(3),GY(2)
	Marnes de Schillersdorf	42 Toarcian	177.5	6	-	D	Ml(70),Li(15),AP(15)
	Couches à *Dactylioceras c.*	41 Toarcian	180	3	-	D	bSh(75),Li(25)
	Schistes carton	40 Toarcian	182	9	-	D	bSh(80),Ml(10),Li(10)
	Calcaire de Kirrwiller	39 Pliensbachian	183.5	1	-	D	Li(85),Ml(15)
	Marnes à *Septaria*	38 Pliensbachian	184.5	7	-	D	Ml(90),Li(35),PY(5)
	Marnes à Ovoïdes	37 Pliensbachian	185.5	52	-	D	id.
	Marnes feuilletées	36 Pliensbachian	186.5	5	-	D	id.
	Calcaire de Zinswiller	35 Pliensbachian	188.5	5	-	D	siLi(80),Ml(20)
	Formation de Bossendorf	34 Pliensbachian	189.5	4	-	D	Ml(100)
	Calcaire de Gundershoffen	33 Sinemurian	191.5	1	-	D	Li(88),Ml(12)
	Formation d'Obermodern	32 Sinemurian	195.5	29	-	D	siLi(80),Ss(5),Si(5),IL(4),PY&Ml(3 ea.)
	Calcaires et Marnes à Gryphées	31 Hettangian	199.5	21	-	D	Ml(40),Li(28),Sh(15),Si(15),KE(2)
	Argiles de Levallois	30 Rhaetian	202	9	-	D	Sh(72),Li(18),Si(5),IL&KAO(2.50 ea.)
	Grès Rhétiens	29 Rhaetian	205	9	-	D	Ss(40),Si(40),Sh(14),Co(5),PY(1)
	Argiles Bariolées dolomitiques	28 Norian	209	27	-	D	siLi(50),Ml(35),Do(15)
	Argiles de Chanville	27 Carnian	227.3	16	-	D	Sh(68),AN(20),Ss(10),Li(2)
	Dolomie de Beaumont	26 Carnian	229	5	-	D	Do(100)
	Argiles Bariolées Intermédiaires	25 Carnian	232	5	-	D	Ml(60),Li(15),Ss(9),Do(5),GY(3)
	Grès à Roseaux	24 Carnian	235	7	-	D	id.
	Marnes Irisées inférieures	23 Carnian	237	97	-	D	Id.
	Dolomie Limite	22 Ladinian	242	1	-	D	Do(100)
	Argiles de la Lettenkohle	21 Anisian	242.5	21	-	D	Sh(35),Si(25),Ss(20),Do(15),doSs(5)
	Dolomie inférieure	20 Anisian	243	11	-	D	Do(50),Sh(25),Si(15),DO(8),GL(2)
	Calcaire à Térébratules	19 Anisian	243.5	2	-	D	Li(80),shLi(20)
	Couches à Cératites	18 Anisian	244	38	-	D	shLi(60),Sh(20),Ml(20)
	Calcaire à Entroques	17 Anisian	244.5	9	-	D	Li(92),Ml(8)
	Dolomie à Lingules	16 Anisian	245	10	-	D	Do(45),Ml(25),Ch(20),CA&CHE(5 ea.)
	Marnes Bariolées	15 Anisian	245.5	37	-	D	AN(50),Ml(30),Do(20)
	Orb.-Schaumkalk-Wellenkalk	14 Anisian	246	14	-	D	shLi(32),Do(23),Sh(22.5),siSh(22.5)
	Wellenmergel-C. Térébratules	13 Anisian	246.5	16	-	D	Ss(26),Do(26),Si(26),DO(7),CA(5)
	Couches à *Myacites*	12 Anisian	247	11	-	D	Si(45),siSh(35),doSs(15), Ml(5)
	Grès Coquillier	11 Olenekian	247.3	8	-	D	doSs(75),Si(15),siSh(10)
	Grès à Voltzia (G. argileux)	10 Olenekian	247.4	9	-	D	Ss(35),shSs(35),Sh(30)
	Grès à Voltzia (G. à Meules)	9 Olenekian	247.5	9	-	D	id.
	Couches Intermédiaires	8 Olenekian	248	41	-	D	doSs(55),siSh(30),Si(10),Do(5)
	Poudingue de Sainte-Odile	7 Olenekian	248.5	20	-	D	Co(100)
	Couches de Karlstal	6 Olenekian	249	100	-	D	Ss(80),Co(20)
	Couches de Rehberg	5 Olenekian	249.5	79	-	D	Ss(60),Co(40)
	Couches de Trifels	4 Olenekian	250	91	-	D	Ss(50),Co(50)
	Gap of Induan	3 Induan	252	-	-	H	-
	Grès d'Annweiler	2 Changhsingian	253	41	-	D	shSs(80),ssSh(20)
	Grès Anté-Annweiler	1 Changhsingian	254	10	-	D	Ss(60),Co(30),Sh(10)
	Top basement	0 Wuchiapingian	259.8				

***Table 2 Input data for the pre-rift burial model of the URG**. Stratigraphic formations and thicknesses from Duringer et al. (2019); Ages in Ma based on the international chrono-stratigraphic chart (Cohen et al., 2013; 2019 revised); Lithological mixes based on the explanatory note of the Haguenau geological map (Ménillet et al., 2015). Abbreviations: E: Erosion; H: Hiatus; D: Deposition; C: Conglomerate; Ss: Sandstone; shSs: Shaly sandstone; doSs: Dolomitic sandstone; Si: Silstone; Sh: Shale; bSh: Black shale; ssSh: Sandy shale; siSh: Silty shale; Li: Limestone; siLi: Silty limestone; shLi: Shaly limestone; Ml: Marls; Do: Dolomite; MI: Mica; PY: Pyrite; GY: Gypsum; KAO: Kaolinite; IL: Illite; CH: Chlorite; AP: Apatite; KE: Kerogen; GL: Glauconite; CA: Calcite; CHE: Chert; DO: dolomite; AN: Anhydrite.*

	EARLY-RIFT MODEL						
	Stratigraphic formation	Modelled layer name	Age (Ma)	Thickness (m)	Eroded thickness (m)	Event type	Lithological Mix (%)
	Marnes Vertes à Limnées	66 Bartonian	39	92	0	D	Ml(70),Ss(12),Co(8),Do(8),AN(2)
	Marnes Calcaires Grises à Anhydrite	65 Bartonian	40	159	0	D	Ml(75),AN(25)
	Zone de transition	64 Lutetian	45	2	0	D	Ml(40),Sh(40),Li(15),PY(5)
	-	63 Selandian	60	-	-460	E	-
DISCUSSED STRATIGRAPHIC CONTRIBUTION	-	62 Maastrichtian	70	-	0	H	-
	-	61 Campanian	80	-	0	H	-
	-	60 Turonian	90	-	0	H	-
	-	59 Cenomanian	100	-	0	H	-
	-	58 Albian	110	-	0	H	-
	-	57 Aptian	120	-	0	H	-
	-	56 Hauterivian	130	-	0	H	-
	-	55 Berriasian	140	-	0	H	-
	-	54 Tithonian	145.1	0	75	D	Li(50),Ml(30),Sh(10),Si(10)
	-	53 Tithonian	150	0	75	D	Li(50),Ml(30),Sh(10),Si(10)
	-	52 Kimmeridgian	155	0	75	D	Li(50),Ml(30),Sh(10),Si(10)
	-	51 Oxfordian	160	0	75	D	Li(50),Ml(30),Sh(10),Si(10)
	Not differentiated	50 Callovian	165	0	60	D	Ml(50),Sh(20),Si(10),Sh(10),Ss(10)
	Not differentiated	49 Bathonian	167	0	50	D	Ml(35),Sh(25),Si(15),Li(10),Ss(10),Sh(5)
	Grande Oolithe	48 Bajocian	169	0	50	D	shLi(72),Sh(26),PY(2)
	INTEGRATION OF THE SYNTHETIC REFERENCE STRATIGRAPHIC COLUMN						

Table 3 Input data for the early-rift burial model of the URG. *Stratigraphic formations and thicknesses after Duringer et al. (2019); Ages in Ma are based on the international chrono-stratigraphic chart (Cohen et al., 2013; 2019 revised); Lithological mixes based on the explanatory note of the Haguenau geological map (Ménillet et al., 2015). Abbreviations: E: Erosion; H: Hiatus; D: Deposition; Co: Conglomerate; Ss: Sandstone; Si: Silstone; Sh: Shale; Li: Limestone; shLi: Shaly limestone; Ml: Marls; Do: Dolomite; PY: Pyrite; AN: Anhydrite*.

5 Results

5.1 Geochemical characteristics of source rock samples

The characteristics of the source rocks in this sample set can be summarized as follows: the Hettangian/Sinemurian Formation (Calcaire et marnes à Gryphées - Lias α; TOC range 2.06-2.9 %; HI range 505-561 mgHCs/gTOC) and the Toarcian Posidonia Shale (Schistes carton - Lias ε; TOC range 0.96-8.03 %; HI range 471-733 mgHCs/gTOC) (**Figure 3**; Ronov, 1958; Tissot et al., 1974; Katz, 1995). Organic matter in these samples is well-preserved type II (marine) kerogen. For the other samples of Jurassic and Triassic ages, the TOC values are <1 % with HI values that do not exceed 125 mgHCs/TOC. An exception is the Muschelkalk limestone for which the HI= 245 mgHCs/gTOC.

Organic matter preservation was also examined using the molecular geochemistry of aliphatic and aromatic fractions determined by GC-MS, especially regarding rocks with low TOC contents. All samples showed well-preserved hydrocarbon distributions (**Figure 4** and **Figure 5**; data not shown except for Toarcian and Hettangian/Sinemurian samples).

5.2 Thermal maturity of rock samples

Hydrogen Index values as a function of T_{max} (°C) are shown in **Figure 3**c. Most samples have T_{max} values below 435 °C and are immature (Peters, 1986). For the Pliensbachian samples, the values cluster around 440 °C and TOC values are lower than <1 %.

Biomarker maturity ratios using hopanes (**Figure 4** and **Table 1**) and steranes (**Figure 5** and **Table 1**) were calculated on *m/z* 191 and *m/z* 217 chromatograms. Specific ratios included: βα/(αβ+ βα) C_{30} hopanes ratio (C_{21} isomerization); S/(S+R) ratios for C_{31} and C_{32} homohopanes (C_{22} isomerization); ββ/(ββ+αα) C_{29} steranes ratio; and S/(S+R) C_{29} 5α(H),14α(H),17α(H) steranes ratio (C_{20} isomerization).

The βα/(αβ+βα) C_{30} hopanes ratios for these samples are distributed over a wide range within the same formation (**Table 1**). These results and those from the ββ/(ββ+αα) C_{29} steranes ratio do not show any correlation with depth. In contrast, 22S/(22S+22R) C_{31} and C_{32} homohopane ratios (**Table 1**) increase respectively from 22 to 60 % and 18 to 61 % following the stratigraphic age of the deposits (and hence paleo-depth) from Liassic to Muschelkalk (**Table 1**; **Figure 6**). However, the C_{32} homohopane ratio results display a discrepancy between Argiles de Levallois Formation (Rhaetian) and Muschelkalk. The 20S/(20S+20R) C_{29} ααα steranes ratio increases from 14 to 45 %, from Liassic to Muschelkalk (**Table 1**; **Figure 6**), following the stratigraphic age of the deposits.

Thermal maturity of the Lutetian sediments in the Saverne Fracture Field (for which no outcrops are currently available) could be estimated from Arpino (1973). The *m/z* 191 chromatogram of lignite from the Complexe Inférieur argileux de Bouxwiller Formation when compared with the Messel shale (e.g., Kimble et al., 1974; Sugden and Abbott, 2002; Adam and Schaeffer, personal communication) has a very low abundance of the C_{31} homohopane S-configuration compared to the R-configuration. The estimated 22S/(22S+22R) C_{31} homohopane ratio (based on Arpino (1973); Adam and Schaeffer, personal communication) is equal to 1.2 %.

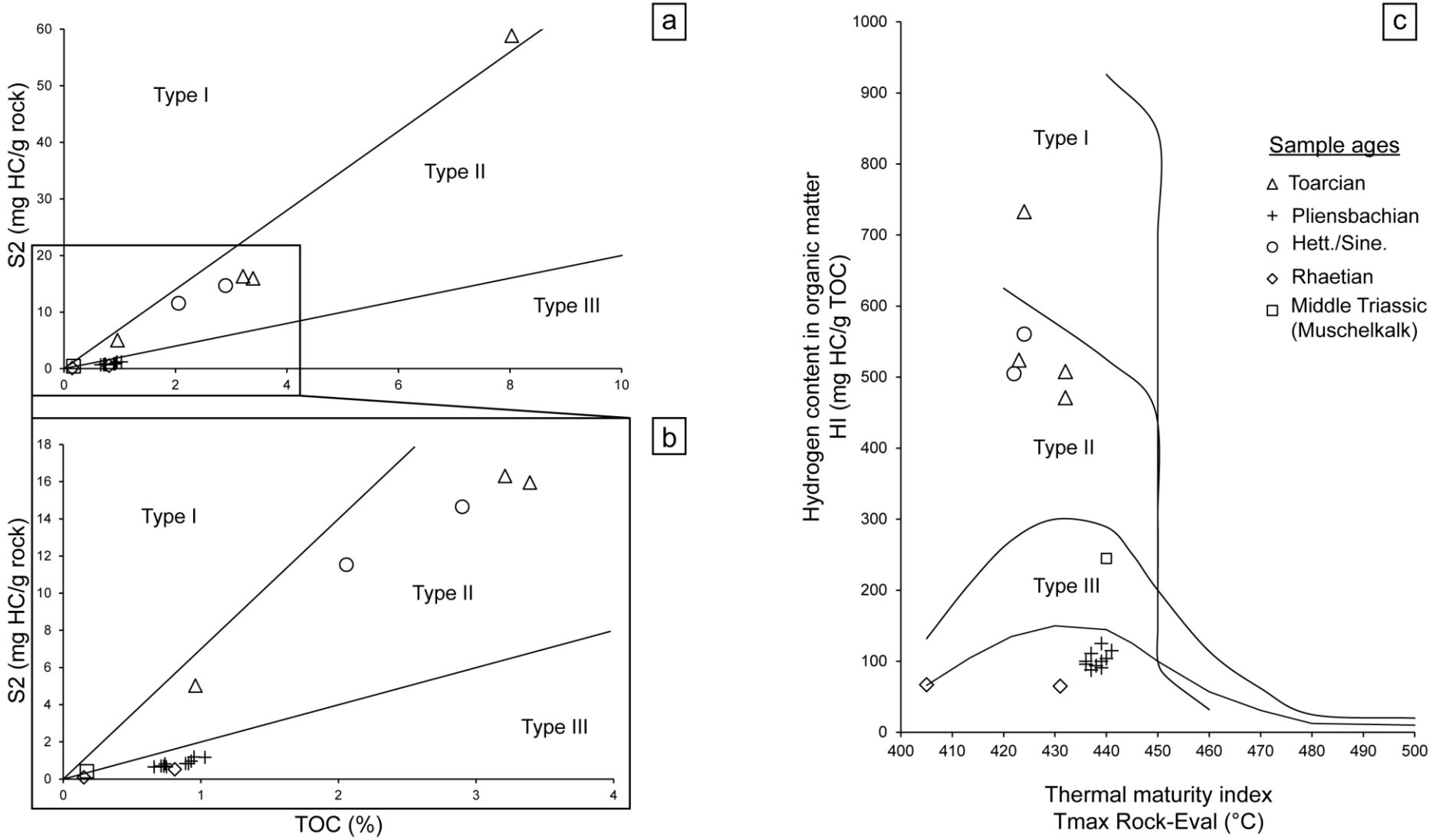

Figure 3 Rock-Eval data of outcrop samples collected in the Saverne Fracture Field. *a. Plot of S2 Rock-Eval (mg HC/g rock) versus TOC (%) indicating kerogen types (Late Triassic sample not indicated). b. Zoom of plot 3a for TOC<4%. c. Plot of Hydrogen Index (mg HC/g TOC) versus T_{max} Rock-Eval (°C) indicating kerogen types and thermal maturity. Same legend for all illustrations.*

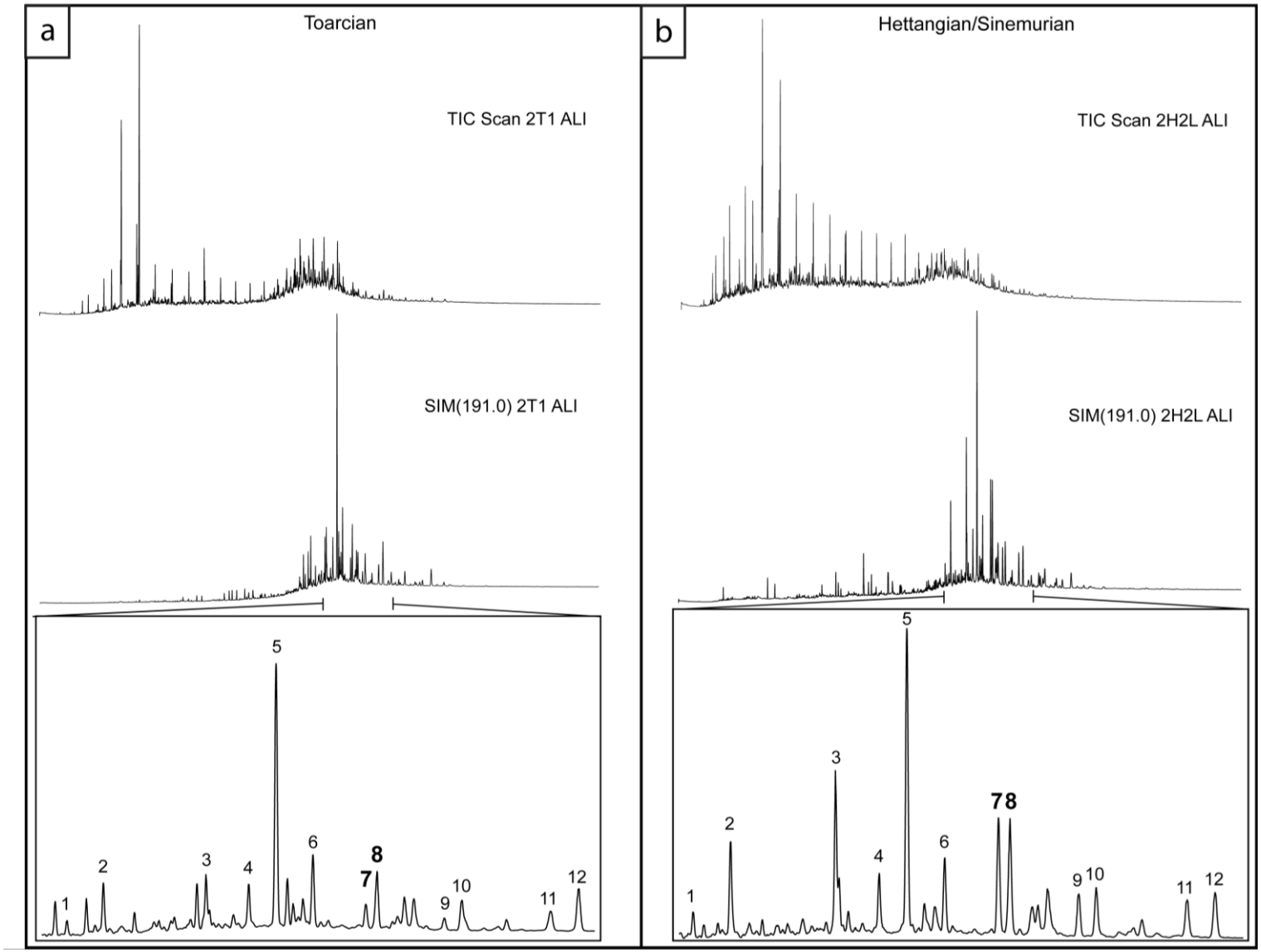

Figure 4 Saturated fractions gas chromatograms (TIC: Fullscan Total Ion chromatogram; SIM m/z 191: Selected ion chromatogram, and partial m/z 191 showing the distributions of hopanes of selected outcrop samples.

a. Toarcian sample 2T1

b. Hettangian/Sinemurian sample 2H2L

Peak assignments:

1: 18α(H),22,29,30-Trisnorneohopane (Ts);

2: 17α(H), 22,29,30-Trisnorhopane (Tm);

3: 17α(H), 21β(H)-30-Norhopane (C_{29} αβ);

4: 17β(H), 21α(H)-30-Norhopane (C_{29} βα);

5: 17 α(H), 21β(H)-Hopane (C_{30} αβ);

6: 17 β(H), 21α(H)-Hopane (C_{30} βα);

7: 17α(H), 21β(H)-22S homohopane (C_{31} αβ S);

8: 17α(H), 21β(H)-22R homohopane (C_{31} αβ R);

9: 17 α(H), 21β(H)-22S bis-homohopane (C_{32} αβ S);

10: 17 α(H), 21β(H)-22R bis-homohopane (C_{32} αβ R);

11: 17 α(H), 21β(H)-22S tris-homohopane (C_{33} αβ S);

12: 17 α(H), 21β(H)-22R tris-homohopane (C_{33} αβ R).

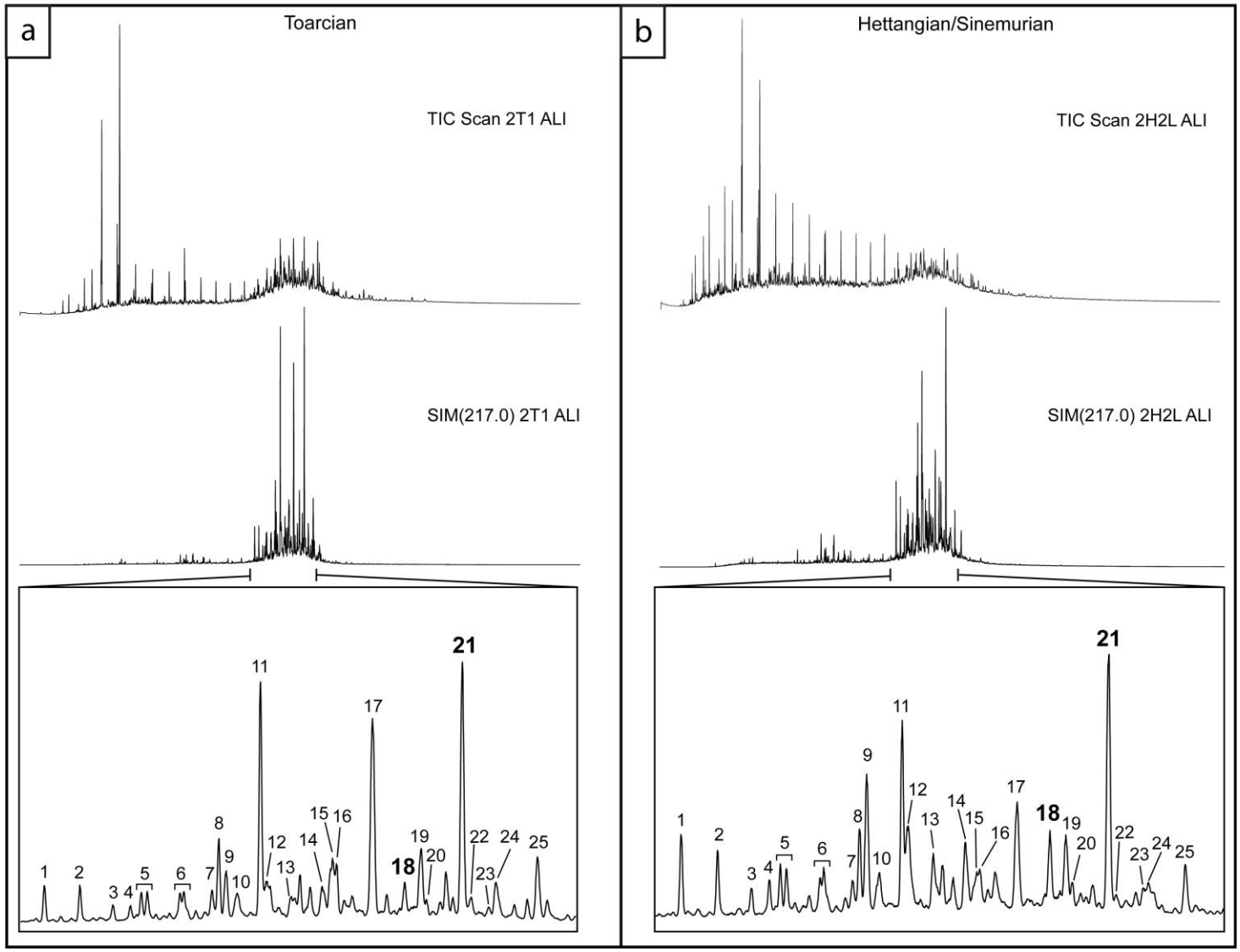

Figure 5 Saturated fractions gas chromatograms (TIC: Fullscan Total Ion chromatogram; SIM m/z 217: Selected ion chromatogram, and partial m/z 217 showing the distributions of steranes of selected outcrop samples.

5a: Toarcian sample 2T1
5b: Hettangian/Sinemurian sample 2H2L
Peak assignments:
1: C_{27} βα 20S
2: C_{27} βα 20R
3: C_{27} αβ 20S
4: C_{27} αβ 20R
*5: C_{28} βα 20S**
*6: C_{28} βα 20R**
7: C_{28} αβ 20S
8: C_{27} ααα 20S
9: C_{27} αββ 20R+C_{29} βα 20S
*10: C_{27} αββ 20S+C_{28} αβ 20R**
11: C_{27} ααα 20R
12: C_{29} βα 20R
13: C_{29} αβ 20S
*14: C_{28} ααα 20S**
15: C_{28} αββ 20R
16: C_{28} αββ 20S
17: C_{28} ααα 20R
18: C_{29} ααα 20S
19: C_{29} αββ 20R
20: C_{29} αββ 20S
21: C_{29} ααα 20R
22: C_{30} ααα 20S
23: C_{30} αββ 20R
24: C_{30} αββ 20S
25: C_{30} ααα 20R
βα, αβ, ααα and αββ denote 13β(H),17α(H)-diasteranes, 13α(H),17β(H)-diasteranes, 5α(H),14α(H),17α(H)-steranes and 5α(H),14β(H),17β(H)-steranes, respectively.
**isomeric peaks (24S and 24R).*

PRE-RIFT MODEL							EARLY-RIFT MODEL			
Strategy No.1: Estimation of the maximum depth of paleoburial by adding eroded sediment thicknesses				**Strategy No.2**: Assignment of the estimated maximum cumulative thickness to the Upper Jurassic and/or Cretaceous			**Strategy No.3**: Consideration of the burial and thermal histories of the early-rift period (Lutetian-Bartonian)			
Simula--tion Results	Simulated curves		Synthesis of simulation tests	Simula--tion Results	Simulated curves		Synthesis of simulation tests	Simula--tion Results	Simulated curves		Synthesis of simulation test
	Run nb.	Color			Run nb.	Color			Run nb.	Color	
Figure 6a, using **S/(S+R) C_{31} H**	1	Orange	Adding 0 m of Malm (160-145.1 Ma) followed by a hiatus period (140-70 Ma), ended by the partial erosion of Bajocian (50 m) and complete erosion of Bathonian, Callovian and Malm in the Paleocene (60-50 Ma)	Figure 6c, using **S/(S+R) C_{31} H**	1	Red	Adding a gradual deposition of 200 m of Malm (160-145.1) and 100 m of Cretaceous (140-70 Ma), followed by the partial erosion of Bajocian (50 m) and complete erosion of Bathonian, Callovian, Malm and Cretaceous (60-50 Ma)	Figure 7, using **S/(S+R) C_{31} H**	1	Black	Adding 300 m of Malm (160-145.1 Ma) then a hiatus period (140-70 Ma), followed by the partial erosion of Bajocian (50 m) and complete erosion of Bathonian, Callovian, Malm and Cretaceous (60-50 Ma), and finally ended by the addition of 253 m of Middle Eocene sediments (45-40 Ma)
	2	Red	Same as above but considering 100 m of Malm		2	Black	Adding 300 m of Malm (160-145.1 Ma) followed by a hiatus period (140-70 Ma), ended by the partial erosion of Bajocian (50 m) and complete erosion of Bathonian, Callovian, Malm and Cretaceous (60-50 Ma)				
	3	Blue	Same as above but considering 200 m of Malm								
	4	Purple	Same as above but considering 300 m of Malm		3	Green	Adding 200 m of Malm (160-145.1 Ma) followed by an alternation of deposition/erosion episodes of Cretaceous (paleoburial max. of 100 m from 140 to 70 Ma), ended by the partial erosion of Bajocian (50 m) and complete erosion of Bathonian, Callovian, Malm and Cretaceous (60-50 Ma)				
	5	Green	Same as above but considering 400 m of Malm								
Figure 6b, using **S/(S+R) ααα C_{29} S**	1	Orange	Same as in Figure 6a	Figure 6d, using **S/(S+R) ααα C_{29} S**	1	Red	Same as in Figure 6c				
	2	Red	Same as in Figure 6a		2	Black	Same as in Figure 6c				
	3	Blue	Same as in Figure 6a								
	4	Purple	Same as in Figure 6a		3	Green	Same as in Figure 6c				
	5	Green	Same as in Figure 6a								

Table 4 Synthesis of the simulations tested on PetroMod© software and refers to the figures where the associated results are represented. S/(S+R) C_{31} H referred to the 22S/(22S+22R) C_{31} homohopane ratio (%) and S/(S+R) ααα C_{29} S to the 20S/(20S+20R) ααα C_{29} steranes ratio (%), both simulated using Mackenzie and McKenzie (1983) kinetic parameters.

5.3 Pre-rift modelling: Results of the strategies No.1 and No.2

The first step of the study considered only the pre-rift period to evaluate the maximum burial depth reached during the Upper Jurassic and the Cretaceous (**Table 2** and **Table 4**). Since the Malm in the study area was deposited and then eroded, an estimate of its initial thickness is required. Strategy No.1 is represented by the graphs in **Figure 6**a and **Figure 6**b. **Figure 6**a compares measured to modelled values of C_{31} homohopane isomerization ratio (expressed as %) as a function of depth by considering (1) 0 m, (2) 100 m, (3) 200 m, (4) 300 m and (5) 400 m thickness of Malm (**Table 4**). **Figure 6**b compares measured to modelled values of C_{29} ααα 20S/(20S+20R) sterane isomerization ratios (expressed as %) as a function of depth by considering the same Malm thicknesses as previously, i.e., (1) 0 m, (2) 100 m, (3) 200 m, (4) 300 m and (5) 400 m (**Table 4**). The best fit between simulated and measured 22S/(22S+22R) C_{31} homohopane and 20S/(20S+20R) C_{29} ααα steranes ratios versus depth is obtained for a Malm thickness ranging from 200 to 300 m and from 300 to 400 m, respectively. Thus, a value of 300 m of Malm was chosen for further modelling (**Figure 6**c and d; **Figure 7**).

Figure 6c and **Figure 6**d show the three simulated curves of strategy No.2 (**Table 4**). The gradual deposition of sediments during the Malm and Cretaceous is represented by the curve in red; the exclusive deposition of Malm followed by a Cretaceous hiatus period is represented by the second curve in black; and the deposition of Malm followed by an alternating deposition/erosion of Cretaceous by the curve in green (**Figure 6**c and d), according to the simulation strategies described in subsection 4.4 and summarized in **Table 4**. It appears that the three curves are almost indistinguishable.

5.4 Early-rift modelling: Results of the strategy No.3

The modelling results corresponding to the early-rift period are represented by **Figure 7** and **Figure 8**. 253 m of Middle Eocene were added to the pre-rift burial model (black curve in **Figure 6**c and d) which considered 300 m of Malm followed by a hiatus period from 140 to 70 Ma, ended by the complete erosion of Malm, Callovian, Bathonian and the partial erosion of Bajocian (60-50 Ma) (**Table 4**). **Figure 7** presents the values of C_{31} homohopane isomerization ratio (expressed as %) as a function of depth, measured on the Mesozoic formations and estimated for the Bouxwiller lignite (see subsection 5.2).

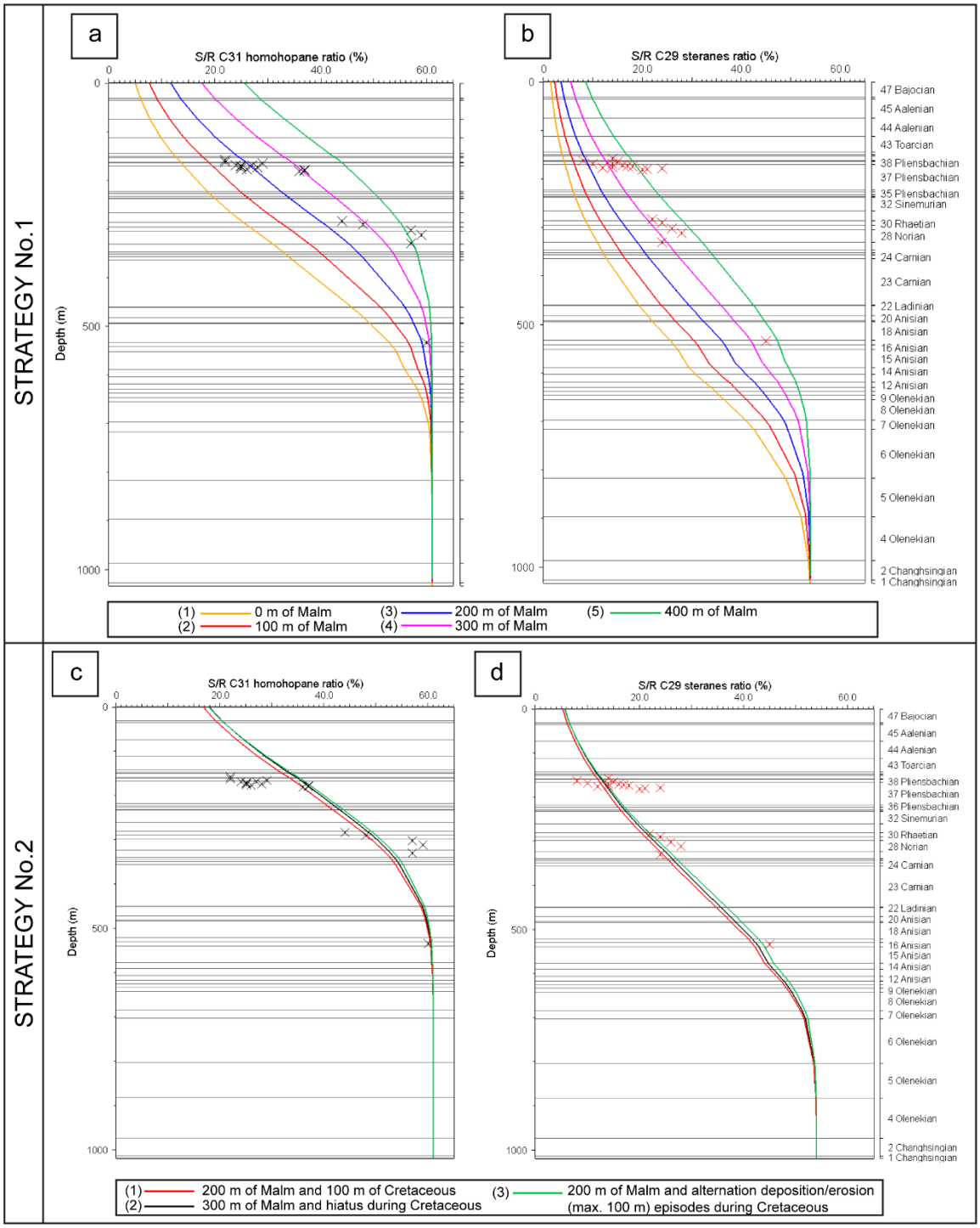

Figure 6 Thermal maturity calibration using modelled (curves) vs. measured (crosses) S/(S+R) ratios (%) versus depth (m) for the strategies No.1 and No.2 using PetroMod© software. *Isomerization kinetic parameters are from Mackenzie and McKenzie (1983). Lithostratigraphic column as in Table 2.* ***a.*** *S/(S+R) C_{31} homohopane ratio (%) evolutions testing 0, 100, 200, 300 and 400 m of Malm (see Table 4).* ***b.*** *S/(S+R) C_{29} steranes ratio (%) versus depth (m) evolutions testing various thicknesses of Malm (same as for 6a; Table 4).* ***c.*** *S/(S+R) C_{31} homohopane ratio (%) versus depth (m) evolutions testing (1)(in red) a gradually deposition from 160 to 70 Ma of 200 m of Malm and 100 m of Cretaceous and subsequent partial erosion of Bajocian and the full erosion of Bathonian, Callovian, Malm and Cretaceous from 60 to 50 Ma; (2)(in black) the deposition of 300 m of Malm followed by a hiatus period from 140 Ma to 70 Ma and subsequent partial erosion of Bajocian and full erosion of the Bathonian, Callovian and Malm from 60 to 50 Ma; (3)(in green) deposition of 200 m of Malm followed by an alternation of deposition/erosion episodes of Cretaceous (paleoburial max. of 100 m) followed by erosion to Bajocian (60-50 Ma).* ***d.*** *S/(S+R) C_{29} steranes ratio (%) versus depth (m) evolutions testing same simulations as in Figure 6c.*

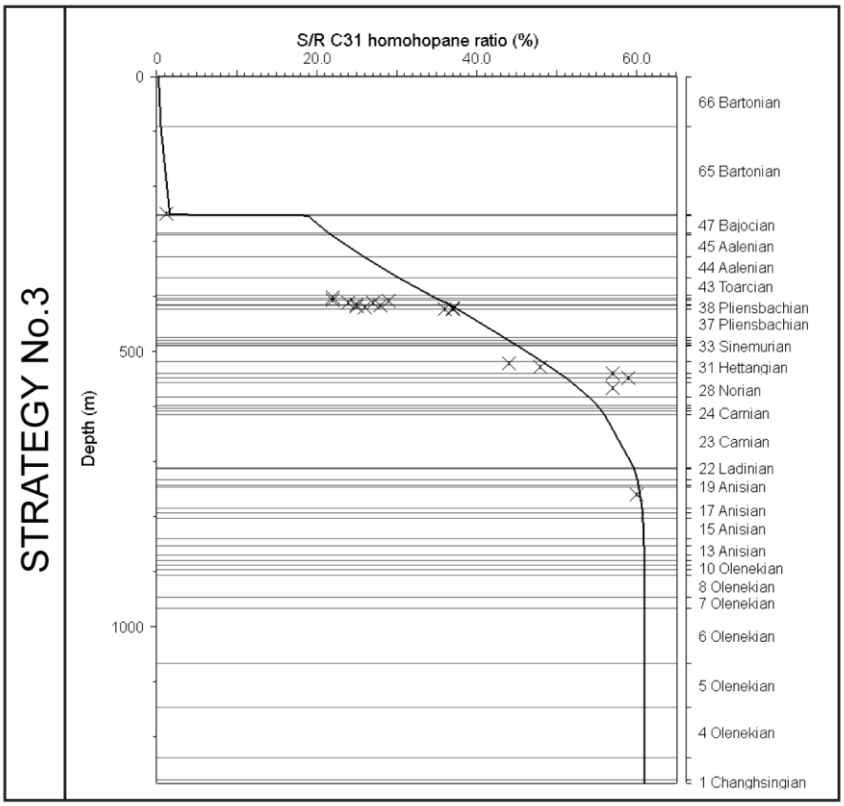

Figure 7 Thermal maturity calibration using modelled (curve) vs. measured (crosses) S/(S+R) C_{31} homohopane ratio (%) versus depth (m) for the strategy No.3 using PetroMod© software. *Isomerization kinetic parameters are from Mackenzie and McKenzie (1983). Lithostratigraphic column as in Table 3. S/(S+R) C_{31} homohopane ratio (%) versus depth (m) evolution based on the simulation represented by the black curve on Figure 6c and d, including deposition of 253 m of Middle Eocene.*

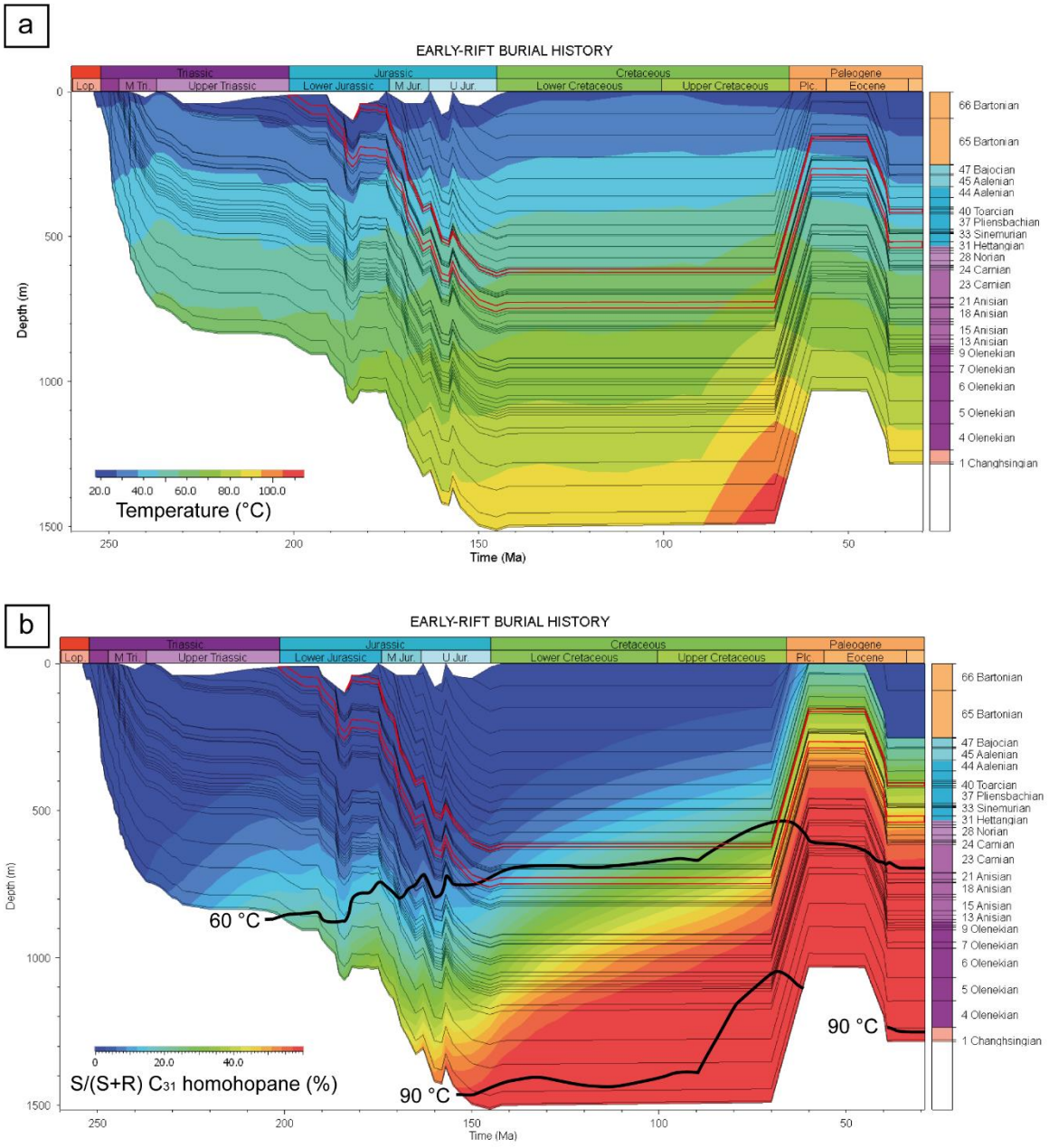

Figure 8 1D basin burial history of the early-rift stage considering the pre-rift model represented by the black curve in Figure 6a and d, followed by the deposition of 253 m of Lutetian and Bartonian according to Duringer et al. (2019) (PetroMod© software)*. a. The two main source rocks are outlined in red and the colored overlay applied correspond to the temperature from 20 to 110 °C. b. The two main source rocks are outlined in red, the isotherms 60 °C and 90 °C are represented by black curves and the colored overlay applied correspond to the simulated thermal maturity of S/(S+R) C_{31} homohopane ratio (%) using Mackenzie and McKenzie (1983) kinetic parameters.*

6 Discussion

6.1 The Saverne Fracture Field source rocks

Rock-Eval pyrolysis results of the Saverne Fracture Field outcrop samples indicate that only the Hettangian/Sinemurian Formation and the Toarcian Posidonia Shale have source rock characteristics (**Table 1**; see subsection 5.1). This conclusion for the Saverne Fracture Field source rocks is similar to Röhl et al. (2001), Frimmel (2003), and Böcker and Littke (2016), who studied source rock properties in the URG. For samples with TOC below 1% (especially the Pliensbachian samples), matrix effects are expected during Rock-Eval pyrolysis and can lead to unreliable T_{max} values (Peters, 1986; Blaise et al., 2011). In addition, variations in the type of OM and its preservation affect T_{max} (Böcker and Littke, 2016), especially for pre-oil window maturity levels (Peters, 1986; di-Giovanni et al., 1998). Yang and Horsfield (2020) list the numerous factors that can influence maturity evaluation using T_{max}. For these reasons, the thermal models were not calibrated using T_{max}.

6.2 Thermal maturity recorded for the Saverne Fracture Field rock samples

No clear correlation was found between maturity and depth concerning ββ/(ββ+αα) C_{29} steranes and βα/(αβ+βα) C_{30} hopane ratios (**Table 1**). The βα/(αβ+βα) C_{30} hopane ratio may be significantly influenced by depositional environment and organic matter input (Moldowan et al., 1986; Rullkötter and Marzi, 1988). The ββ/(ββ+αα) C_{29} steranes ratio is described in the literature as rather independent of organic matter source (Seifert and Moldowan, 1986). Yet, its evolution as a function of thermal maturation is most effective within oil window. Conversely, a good correlation was found between maturity and depth using the 20S/(20S+20R) C_{29} ααα steranes ratio.

At lower maturity levels, homohopanes isomerization occurs earlier than for many other biomarker maturity parameters. The 22S/(22S+22R) homohopanes ratio increases from 0 to an equilibrium value of 55-62 % at onset of oil window (Seifert and Moldowan, 1980; Zumberge, 1987; Marzi, 1992). This ratio when measured on the sample set increases from 22 to 60 %, following the stratigraphic age of the deposits (**Table 1**). Same ranges of thermal maturity values were measured in the corresponding stratigraphic formations of the eastern Paris Basin (Blaise et al., 2011). The variable data for the Triassic clay and sandstone samples are a consequence of a low signal-to-noise ratio related to low biomarker content which led to the overestimation of maturity. In any case, isomerization ratio equilibrium values increase with stratigraphic depth up to 60 % for Triassic which has therefore reached the onset of oil window (**Figure 6**; Seifert and Moldowan, 1980; Zumberge, 1987; Marzi, 1992). The same conclusion is obtained for the 20S/(20S+20R) C_{29} ααα sterane ratios, which increases from 14 to 45 % (**Table 1**). This means that the Liassic petroleum source rocks did not generate oil before the opening of the URG. Their immaturity level is, therefore, a significant constraint to the determination by modelling of the maximum burial depth (reached during the Jurassic/Cretaceous hiatus; **Figure 8**).

6.3 Estimation of the maximum cumulative thickness of Jurassic/Cretaceous eroded sediments

The best fit between measured and modelled data using C_{31} 22S/(22S+22R) homohopane ratio (%) is obtained for a sediment thickness ranging from 200 to 300 m. Meanwhile, the best fit between measured and modelled data using C_{29} 20S/(20S+20R) sterane ratio (%) is obtained for a sediment thickness ranging from 300 to 400 m. This leads to a mean estimated value of 300 m thickness of Malm (**Figure 6**a and b). This thickness is relatively low compared to the approximately 700 m of Malm in the central Paris Basin

(Guillocheau et al., 2000) or approximately 500-550 m in the Southwest German Basin (Thomas and Schulz, 2007). Mazurek et al. (2006) proposed that in the Swiss Molasse Basin, 600-700 m of late Jurassic and Cretaceous sediments were deposited.

In his model (1D thermal model of Mingolsheim 1986 Well, URG), Böcker (2015) speculated a deposit of 400 m of Malm and 200 m of Cretaceous sediments, presumably corresponding to the total cumulative thickness of sediments deposited during the sedimentary hiatus. Thermal modelling allows the estimation of the maximum depth of paleoburial by adding thickness of sediments that thermally impacted the underlying layers, i.e. the maximum cumulative thickness.

If the Cretaceous was deposited, it happened with alternating depositional and erosional periods, as discussed in Böcker (2015) and references therein (e.g., Meyer, 1976; Haq, 2014). In addition, during this period, the study area was uplifted (Cloos, 1939; Illies, 1975) and elevated above the depositional level (Scheck-Wenderoth et al., 2008; Ménillet et al., 2015). Since the "depositional duration" variable strongly impacts the source rock maturation, the total cumulative thickness of Cretaceous sediments is not representative of the maximum cumulative thickness. In addition, as the Upper Jurassic-Early Cretaceous correspond to a Europe-wide sea-level fall, the marine regression resulted in the isolation of depositional basins (Ruffell, 1991), which prevents the straightforward comparison of the Saverne Fracture Field (the future URG area) with the surrounding basins. However, whether the maximum cumulative thickness of about 300 m (**Figure 6**a and b) can be attributed to Malm sediments only or to Malm and Cretaceous needs to be tested.

6.4 Assignment of the estimated maximum cumulative thickness to the Upper Jurassic and/or Cretaceous

Table 4 summarizes simulations testing the hypothesis of Cretaceous deposition: (1) the first simulated curve (red curve in **Figure 6**c and d) corresponds to a gradual deposition of 200 m of Malm and 100 m of Cretaceous (from 160 to 70 Ma), followed by the partial erosion of Bajocian and the complete erosion of Bathonian, Callovian and Malm (from 60 to 50 Ma); (2) the second curve (black curve on **Figure 6**c and d) corresponds to a deposition of 300 m of Malm followed by a hiatus period (from 140 to 70 Ma), and then by the partial erosion of Bajocian and complete erosion of Bathonian, Callovian and Malm (from 60 to 50 Ma); and (3) the third curve (green curve on **Figure 6**c and d) corresponds to a deposition of 200 m of Malm followed by an alternation of deposition/erosion episodes of Cretaceous (maximum cumulative thickness of 100 m), followed by the partial erosion of Bajocian and the complete erosion of Bathonian, Callovian and Malm (from 60 to 50 Ma).

The models based on strategy No.2 testing the hypothesis of Cretaceous deposition show that all the tested burial conditions are consistent with the measured data (**Figure 6**c and d). However, if the Cretaceous deposited, it must not have accumulated significant thicknesses (maximum cumulative thickness ≤ 100 m; simulation results not shown). Indeed, although the Cretaceous exists in the Paris Basin, it is absent in the southwestern part of Germany (Geyer et al., 1991; LGRB, 1998; Lahner and Toloczyki, 2004). Blaise et al. (2011, 2014) estimated its thickness to decrease eastward within Paris Basin. In this sense, it appears that the paleo-shoreline was very likely at the eastern end of the Paris Basin (Ziegler, 1990), at the border of the future URG area in progressive uplift (Cloos, 1939). Given the geodynamics of the Upper Jurassic/Cretaceous period (e.g., Ziegler, 1987; Hibsch et al., 1995), the multiplication of tectonic events and the strong structural inheritance of the study area (Schumacher, 2002; Sissingh, 2006; Edel et al., 2007), the sediments were likely not deposited continuously (as considered for the red curve in **Figure 6**c and d). As mentioned above, for some authors if the Cretaceous was deposited, it happened with alternating depositional and erosional periods. It turns out that the simulation of alternating deposition/erosion of Cretaceous sediments might be accredited regarding the simulation results (green curve on **Figure 6**c and d), although

there is no evidence of Cretaceous deposition and subsequent erosion. For this reason, the estimation of alternating deposited and eroded sediments during Cretaceous is questionable. Because the simulation results are the same, it seems more relevant from a modelling perspective to use the simplest simulation represented by the black curve, i.e., the exclusive deposition of Malm followed by a Cretaceous hiatus period before erosion (black curve in **Figure 6**c). For all simulations, maximum temperatures of the Posidonia Shale and the Hettangian/Sinemurian Formation reached before the onset of the URG are about 65 °C and 72 °C, respectively. These values were reached during Late Cretaceous (70 Ma) (**Figure 8**a).

6.5 Consideration of the burial and thermal histories of the early-rift period

To consider an influence of the very first stages precursor to the URG main onset, the modelling represented in **Figure 7** and **Figure 8** is based on a simulation adding 253 m of early-rift sediments (deduced from the GRT-1 well and in agreement with the presence of sparse Eocene deposits in the Saverne Fracture Field) to the burial history represented by the black curve of **Figure 6**c and **Figure 6**d (see **Table 4**). This modelling corresponds to a sensitivity test of the simplest pre-rift model (black curve on **Figure 6**c and d). Its burial history and the associated evolution of the 22S/(22S+22R) C_{31} homohopane over time is represented in **Figure 8**b. The evolution of this ratio according to depth reveals a shift in the simulated trend between the pre-rift and the early-rift series (**Figure 7**). This is a consequence of the Upper Jurassic/Cretaceous erosion and the transition from pre-rift geothermal history to rift initiation. Such shift is also observed in thermal maturity measurements within wells of the Pechelbronn sub-basin (Robert, 1985; Böcker, 2015; and references therein). For Mesozoic sediments, the considered scenario induces a slight shift towards the higher conversion of 22S/(22S+22R) C_{31} homohopane ratio in response to additional burial and heating during the early-rift, within acceptable range of measured data. The Bouxwiller lignite estimated S/(S+R) C_{31} homohopane value of 1.2 % is in complete agreement with the early-rift sediment thickness of the well GRT-1 (Pechelbronn sub-basin). Note that the approximately 250 m thickness can be attributed actually to Eocene deposits alone or to Eocene deposits plus additional Oligocene alluvial fans, in response to the later activity of the faults (Ménillet et al., 1979; Genre, 1981).

7 Conclusion

This study combining basin burial and thermal modelling, as well as biomarker geochemistry from the Saverne Fracture Field, improves the knowledge of the URG pre-rift and early-rift thermal history. First, the results show that the Liassic source rocks of the Saverne Fracture Field are immature. The 22S/(22S+22R) C_{31} homohopane ratio equilibrium values indicate that the onset of the oil window is reached in the Triassic stratigraphic levels. The thermal maturity measurements calculated from the 22S/(22S+22R) C_{31} homohopane and 20S/(20S+20R) C_{29} ααα steranes ratios were integrated into PetroMod© software as calibration values. The reconstruction of a synthetic reference stratigraphic column for the Saverne Fracture Field and the testing of several burial scenarios and thermal modelling using PetroMod© software proposes a maximum cumulative thickness of 300 m of eroded sediments above the Dogger series. In contrast, it could not be demonstrated whether this value should be attributed to Malm deposits solely or to Malm and Cretaceous. However, in regards to literature and burial sensitivity tests, the maximum cumulative thickness of Cretaceous must have been low (≤ 100 m). These conclusions can be transposed to the eastern Paris Basin, which recorded the same thermal history from the Permian to the Cretaceous/Paleocene. In addition, the thermal maturity measurement of the Bouxwiller Lutetian lignites combined with thermal modelling indicates that, during the very first onset of the URG, the Mesozoic sediments could have been buried again by about 250 m of Cenozoic sediments, with negligible influence on the pre-rift thermal signature. As a consequence, the thermal maturity of the Liassic source rocks within the URG was never sufficient to reach the oil window during the pre-rift stage. Their maturation in the deeper parts of the URG to reach the oil-to-gas windows would then only be the consequence of syn-rift to post-rift burial, with the potential (local) additional influence of geothermal anomalies. Thanks to this study, the determination of their respective contribution to the overall thermal effect on the URG source rocks can now be further investigated.

ACKNOWLEDGEMENTS

The authors would like to thank ÉS-Geothermie and especially A. Genter for sharing their data on well GRT-1 and scientific discussions, as well as P. Adam and P. Schaeffer (University of Strasbourg) for sharing GC-MS data on the aliphatic fraction of the Messel shale. We also thank Schlumberger for providing the PetroMod© academic license. Dr. B. Katz and T. Blaise are thanked for their thorough and detailed review as well as Prof. P. Philp for English spelling and clarity advisory. Their respective contributions greatly improved our manuscript. The Université de Lorraine is acknowledged for funding this research through the “Lorraine Université d’Excellence” initiative (DEEPSURF project), reference ANR-15-IDEX-04-LUE.

8 References

Abuhelou, F., Mansuy-Huault, L., Lorgeoux, C., Catteloin, D., Collin, V., Bauer, A., Kanbar, H.J., Gley, R., Manceau, L., Thomas, F., 2017. Suspended particulate matter collection methods influence the quantification of polycyclic aromatic compounds in the river system. Environmental Science and Pollution Research 24(28), 22717–22729.

Arpino, P., 1973. Les lipides de sédiments lacustres éocènes. Doctoral Dissertation, Université de Strasbourg, 107 pp.

Baillieux, P., Schill, E., Edel, J.-B., Mauri, G., 2013. Localization of temperature anomalies in the Upper Rhine Graben: insights from geophysics and neotectonic activity. International Geology Review 55(14), 1744–1762.

Bajor, M., Roquebert, M., Van der Weide, B., 1969. Transformation de la matiere organique sedimentaire sous l'influence de la temperature. Bull. Centre Recherches Pau–SNPA 3(1), 113–124.

Baujard, C., Genter, A., Dalmais, E., Maurer, V., Hehn, R., Rosillette, R., Vidal, J., Schmittbuhl, J., 2017. Hydrothermal characterization of wells GRT-1 and GRT-2 in Rittershoffen, France: Implications on the understanding of natural flow systems in the Rhine Graben. Geothermics 65, 255–268.

Berger, J.-P., Reichenbacher, B., Becker, D., Grimm, M., Grimm, K., Picot, L., Storni, A., Pirkenseer, C., Derer, C., Schaefer, A., 2005. Paleogeography of the upper Rhine Graben (URG) and the Swiss Molasse basin (SMB) from Eocene to Pliocene. International Journal of Earth Sciences 94(4), 697–710.

Biache, C., Lorgeoux, C., Andriatsihoarana, S., Colombano, S., Faure, P., 2015. Effect of pre-heating on the chemical oxidation efficiency: implications for the PAH availability measurement in contaminated soils. Journal of hazardous materials 286, 55–63.

Blaise, T., 2012. Histoire thermique et interactions fluides-roches dans l'Est du Bassin de Paris. Doctoral Dissertation, Université de Lorraine, 348 pp.

Blaise, T., Barbarand, J., Kars, M., Ploquin, F., Aubourg, C., Brigaud, B., Cathelineau, M., El Albani, A., Gautheron, C., Izart, A., Janots, D., Michels, R., Pagel, M., Pozzi, J.-P., Boiron, M.-C., Landrein, P., 2014. Reconstruction of low temperature (< 100 C) burial in sedimentary basins: a comparison of geothermometer in the intracontinental Paris Basin. Marine and Petroleum Geology 53, 71–87.

Blaise, T., Izart, A., Michels, R., Suarez-Ruiz, I., Cathelineau, M., Landrein, P., 2011. Vertical and lateral changes in organic matter from the Mesozoic, eastern Paris Basin (France): variability of sources and burial history. International journal of coal geology 88(2-3), 163–178.

Böcker, J., 2015. Petroleum system and thermal history of the Upper Rhine Graben: Implications from organic geochemical analyses, oil-source rock correlations and numerical modelling. Doctoral Dissertation, Fakultät für Georessourcen und Materialtechnik der Rheinisch -Westfälischen Technischen Hochschule Aachen, 104 pp.

Böcker, J., Littke, R., 2016. Thermal maturity and petroleum kitchen areas of Liassic Black Shales (Lower Jurassic) in the central Upper Rhine Graben, Germany. International Journal of Earth Sciences 105(2), 611–636.

Böcker, J., Littke, R., Forster, A., 2016. An overview on source rocks and the petroleum system of the central Upper Rhine Graben. International Journal of Earth Sciences 106(2), 707–742.

Boigk, H., Schöneich, H., 1970. Die Tiefenlage der Permbasis im nördlichen Teil des Oberrheingrabens. Graben problems 27, 48–55.

Bossennec, C., 2019. Évolution des propriétés de transfert des grès par diagénèse et déformation: application aux formations du Buntsandstein Gp., Graben du Rhin. Doctoral Dissertation, Université de Lorraine, 580 pp.

Bossennec, C., Géraud, Y., Böcker, J., Klug, B., Mattioni, L., Sizun, J.-P., Sudo, M., Moretti, I., 2021. Evolution of diagenetic conditions and burial history in Buntsandstein Gp. fractured sandstones (Upper Rhine Graben) from in-situ δ18O of quartz and 40Ar/39Ar geochronology of K-feldspar overgrowths. International Journal of Earth Sciences 110(8), 2779–2802.

Bourgeois, O., Ford, M., Diraison, M., Veslud, C., Gerbault, M., Pik, R., Ruby, N., Bonnet, S., 2007. Separation of rifting and lithospheric folding signatures in the NW-Alpine foreland. International Journal of Earth Sciences 96(6), 1003–1031.

Bourquin, S., Guillocheau, F., 1996. Keuper stratigraphic cycles in the Paris Basin and comparison with cycles in other Peritethyan basins (German Basin and Bresse-Jura Basin). Sedimentary geology 105(3-4), 159–182.

Bourquin, S., Guillocheau, F., Péron, S., 2009. Braided rivers within an arid alluvial plain (example from the Lower Triassic, western German Basin): recognition criteria and expression of stratigraphic cycles. Sedimentology 56(7), 2235–2264.

Bourquin, S., Peron, S., Durand, M., 2006. Lower Triassic sequence stratigraphy of the western part of the Germanic Basin (west of Black Forest): fluvial system evolution through time and space. Sedimentary Geology 186(3-4), 187–211.

Bourquin, S., Robin, C., Guillocheau, F., Gaulier, J.-M., 2002. Three-dimensional accommodation analysis of the Keuper of the Paris Basin: discrimination between tectonics, eustasy and sediment supply in the stratigraphic record. Marine and Petroleum Geology 19(4), 469–498.

Briais, J., Lasseur, E., Homberg, C., Beccaletto, L., Couëffé, R., Bellahsen, N., Chateauneuf, J.-J., 2017. Sedimentary record and structural analysis of the opening of the European Cenozoic Rift System: The case of the Upper Rhine Graben. Presented at the EGU General Assembly Conference Abstracts, p. 17227.

Bruns, B., Littke, R., Gasparik, M., van Wees, J., Nelskamp, S., 2016. Thermal evolution and shale gas potential estimation of the Wealden and Posidonia Shale in NW-Germany and the Netherlands: a 3D basin modelling study. Basin Research 28(1), 2–33.

Bruss, D., 2000. Zur Herkunft der Erdoele im mittleren Oberrheingraben und ihre Bedeutung fuer die Rekonstruktion der Migrationsgeschichte und der Speichergesteinsdiagenese. Doctoral Dissertation, Universität Erlangen-Nürnberg, Forschungszentrum Jülich. Berichte des Forschungszentrums Jülich, 3831, 222 pp.

Buchmann, T.J., Connolly, P.T., 2007. Contemporary kinematics of the Upper Rhine Graben: A 3D finite element approach. Global and Planetary Change 58(1-4), 287–309.

Burrus, J., 1986. Thermal Modeling in Sedimentary Basins: 1st IFP Exploration Research Conference, Carcans, France, June 3-7, 1985. Editions Technip.

Chantraine, J., Autran, A., Cavelier, C., Alabouvette, B., Barféty, J., Cecca, F., Clozier, L., Debrand-Passard, S., Dubreuilh, J., Feybesse, J., 1996. Carte géologique de la France à 1/1 000 000. BRGM Orléans ed.

Châteauneuf, J.-J., Ménillet, F., 2014. Découverte d'une microflore bartonienne dans le Fossé rhénan supérieur: la formation de Mietesheim (Bas-Rhin, Alsace, France). Géologie de la France (1), 3–20.

Cloethingh, S., Ziegler, P.A., 2007. Tectonic Models for the Evolution of Sedimentary Basins, in Crust and Lithosphere Dynamics. In: Watts, A.B. (eds) Treatise on Geophysics, 486–611.

Cloos, H., 1939. Hebung-Spaltung-Vulkanismus, Elemente einer geomet-risch en Analyse irdischer Grossformen. Geol. Rund. 30, 406–527.

Cohen, K.M., Finney, S.C., Gibbard, P.L., Fan, J.-X., 2013 (updated). The ICS international chronostratigraphic chart. Episodes 36, 199–204.

Curnelle, R., Dubois, P. (1986). Évolution mésozoique des grands bassins sédimentaires Français; bassins de Paris, d'Aquitaine et du Sud-Est. Bulletin de la Société géologique de France 2(4), 529-546.

Derer, C.E., 2003. Tectono-sedimentary evolution of the northern Upper Rhine Graben (Germany), with special regard to the early syn-rift stage. Doctoral dissertation, Rheinischen Friedrich-Wilhelms-Universität Bonn, 103 pp.

Derer, C.E., Schumacher, M.E., Schäfer, A., 2005. The northern Upper Rhine Graben: basin geometry and early syn-rift tectono-sedimentary evolution. International Journal of Earth Sciences 94(4), 640–656.

Dèzes, P., Schmid, S.M., Ziegler, P.A., 2004. Evolution of the European Cenozoic Rift System: interaction of the Alpine and Pyrenean orogens with their foreland lithosphere. Tectonophysics 389(1-2), 1–33.

di-Giovanni, C., Disnar, J.R., Bichet, V., Campy, M., Guillet, B., 1998. Geochemical characterization of soil organic matter and variability of a postglacial detrital organic supply (Chaillexon Lake, France). Earth Surface Processes and Landforms: The Journal of the British Geomorphological Group 23(12), 1057–1069.

Donsimoni, M., 1981. Le bassin houiller lorrain: Synthèse géologique. Mém. BRGM, Orléans, 117, 102 pp.

Duringer, P., 1988. Les conglomérats des bordures du rift Cénozoïque Rhénan. Dynamique sédimentaire et contrôle climatique. Doctoral Dissertation, Université de Strasbourg, 328 pp.

Duringer, P., Aichholzer, C., Orciani, S., Genter, A., 2019. The complete lithostratigraphic section of the geothermal wells in Rittershoffen (Upper Rhine Graben, eastern France): a key for future geothermal wells. BSGF-Earth Sciences Bulletin 190(1), 13.

Edel, J., Fluck, P., 1989. The upper Rhenish Shield basement (Vosges, Upper Rhinegraben and Schwarzwald): main structural features deduced from magnetic, gravimetric and geological data. Tectonophysics 169(4), 303–316.

Edel, J.-B., Schulmann, K., Rotstein, Y., 2007. The Variscan tectonic inheritance of the Upper Rhine Graben: evidence of reactivations in the Lias, Late Eocene–Oligocene up to the recent. International Journal of Earth Sciences 96(2), 305–325.

Équipe du projet GeORG (2013). Potentiel géologique profond du Fossé rhénan supérieur. Rapport scientifique et technique du projet Interreg GeORG, Part 1-4; Internet (PDF-document: http://www.geopotenziale.eu).

Frey, M., Bär, K., Stober, I., Reinecker, J., van der Vaart, J., Sass, I., 2022a. Assessment of deep geothermal research and development in the Upper Rhine Graben. Geothermal Energy 10, 1–67.

Frey, M., van der Vaart, J., Bär, K., Bossennec, C., Calcagno, P., Dezayes, C., Sass, I., 2022b. Techno-Economic Assessment of Geothermal Resources in the Variscan Basement of the Northern Upper Rhine Graben. Natural Resources Research 1–22.

Fries, D., Lebouil, S., Maurer, V., Martin, C., Baujard, C., Ravier, G., Boguais, R., Amari, S., 2022. Lithium extraction through pilot scale tests under real geothermal conditions of the Upper Rhine Graben. Presented at the Proceedings European Geothermal Congress, p. 7.

Frimmel, A., 2003. Hochauflösende Untersuchungen von Biomarkern an epikontinentalen Schwarzschiefern des Unteren Toarciums (Posidonienschiefer, Lias ε [Lias-epsilon]) von SW-Deutschland. Doctoral dissertation, Eberhard-Karls-Universität Tübingen, 109 pp.

Gallagher, K., Evans, E., 1991. Estimating kinetic parameters for organic reactions from geological data: an example from the Gippsland Basin, Australia. Applied geochemistry 6(6), 653–664.

Genre, C., 1981. BRGM Carte géologique de la France au 1: 50 000 Feuille Saverne. Norois 110(1), 237–238.

Gérard, A., Kappelmeyer, O., 1987. The Soultz-sous-Forêts project. Geothermics 16(4), 393–399.

Geyer, O.F., Gwinner, M.P., Geyer, M., Nitsch, E., Simon, T., 1991. Geologie von baden-Württemberg, Schweizerbart, Stuttgart, Germany, 472 pp.

Grimmer, J., Ritter, J., Eisbacher, G., Fielitz, W., 2017. The late Variscan control on the location and asymmetry of the Upper Rhine Graben. International Journal of Earth Sciences 106(3), 827–853.

Guillocheau, F., Robin, C., Allemand, P., Bourquin, S., Brault, N., Dromart, G., Friedenberg, R., Garcia, J.-P., Gaulier, J.-M., Gaumet, F., 2000. Meso-Cenozoic geodynamic evolution of the Paris Basin: 3D stratigraphic constraints. Geodinamica Acta 13(4), 189–245.

Hantschel, T., Kauerauf, A.I., 2009. Fundamentals of basin and petroleum systems modeling. Springer Science & Business Media, 476 pp.

Haq, B.U., 2014. Cretaceous eustasy revisited. Global and Planetary change 113, 44–58.

Hautevelle, Y., Michels, R., Malartre, F., Trouiller, A., 2006. Vascular plant biomarkers as proxies for palaeoflora and palaeoclimatic changes at the Dogger/Malm transition of the Paris Basin (France). Organic Geochemistry 37(5), 610–625.

Hibsch, C., Jarrige, J.-J., Cushing, E.M., Mercier, J., 1995. Palaeostress analysis, a contribution to the understanding of basin tectonics and geodynamic evolution. Example of the Permian/Cenozoic tectonics of Great Britain and geodynamic implications in western Europe. Tectonophysics 252(1-4), 103–136.

Hinsken, S., Ustaszewski, K., Wetzel, A., 2007. Graben width controlling syn-rift sedimentation: the Palaeogene southern Upper Rhine Graben as an example. International Journal of Earth Sciences 96(6), 979–1002.

Illies, J., 1975. Recent and paleo-intraplate tectonics in stable Europe and the Rhinegraben rift system. In: Developments in Geotectonics. Elsevier 9, 251–264.

Katz, B.J., 1995. Petroleum source rocks—An introductory overview. In: Katz, B.J. (eds) Petroleum Source Rocks. Casebooks in Earth Sciences. Springer, Berlin, Heidelberg, 1–8.

Kimble, B., Maxwell, J., Philp, R., Eglinton, G., Albrecht, P., Ensminger, A., Arpino, P., Ourisson, G., 1974. Tri-and tetraterpenoid hydrocarbons in the Messel oil shale. Geochimica et Cosmochimica Acta 38(7), 1165–1181.

Kohl, T., Bächler, D., Rybach, L., 2000. Steps towards a comprehensive thermo-hydraulic analysis of the HDR test site Soultz-sous-Forêts. Presented at the Proceedings World Geothermal Congress, Kyushu-Tohoku Japan, 2671–2676.

Kupecz, J.A., Gluyas, J., Bloch, S., 1997. Reservoir quality prediction in sandstones and carbonates: An overview. AAPG Memoir 69, VII-XXIV.

Lahner, L., Toloczyki, M., 2004. Geowissenschaftliche Karte der Bundesrepublik Deutschland 1: 2.000. 000. Geologie, Bundesanstalt für Geowissenschaften und Rohstoffe, Hannover.

Landais, P., Elie, M., 1999. Utilisation de la géochimie organique pour la détermination du paléoenvironnement et de la paléothermicité dans le Callovo-Oxfordien du site de l'Est de la France. EDP Sciences 1999, 35–58.

Landrein, P., Vigneron, G., Delay, J., Lebon, P., Pagel, M., 2013. Lithologie, hydrodynamisme et thermicité dans le système sédimentaire multicouche recoupé par les forages Andra de Montiers-sur-Saulx (Meuse). Bulletin de la Société géologique de France 184(6), 519–543.

Lardeaux, J., Schulmann, K., Faure, M., Janoušek, V., Lexa, O., Skrzypek, E., Edel, J., Štípská, P., 2014. The moldanubian zone in the French Massif Central, Vosges/Schwarzwald and Bohemian Massif revisited: differences and similarities. Geological Society, London, Special Publications 405(1), 7–44.

Laubscher, H., 1987. Die tektonische Entwicklung der Nordschweiz. Eclogae Geologicae Helvetiae 80(2), 287–303.

Le Meur, M., Boussafir, M., Le Milbeau, C., Debure, M., Claret, F., Robinet, J.-C., Lerouge, C., 2021. Organic Matter Oxidation of the Tégulines Clay formation, (Paris Basin, France): Spatial Heterogeneities. Applied Geochemistry 134, 105093.

Le Roux, J., Harmand, D., 2003. Origin of the Hydrographic network in the Eastern Paris Basin and its border massifs. Géologie de la France 1, 105–110.

LGRB, 1998. Geologische Übersichtskarte von Baden-Württemberg 1:300,000 (GÜ 300) [Geological map of the state of Baden-Württemberg 1:300,000]. Landesamt für Geologie, Rohstoffe und Bergbau Baden-Württemberg (LGRB).

Li, Y., Michels, R., Mansuy, L., Fleck, S., Faure, P., 2002. Comparison of pressurized liquid extraction with classical solvent extraction and microwave-assisted extraction–application to the investigation of the artificial maturation of Mahakam coal. Fuel 81(6), 747–755.

Littke, R., Bayer, U., Gajewski, D., Nelskamp, S. (eds) 2008. Dynamics of complex intracontinental basins: the central European basin system. Springer, 227–290.

Lutz, H., Lorenz, V., Engel, T., Häfner, F., Haneke, J., 2013. Paleogene phreatomagmatic volcanism on the western main fault of the northern Upper Rhine Graben (Kisselwörth diatreme and Nierstein–Astheim Volcanic System, Germany). Bulletin of Volcanology 75(7), 1–11.

Lutz, M., Cleintuar, M., 1999. Geological results of a hydrocarbon exploration campaign in the southern Upper Rhine Graben (Alsace Centrale, France). Bulletin für angewandte Geologie 4, 3–80.

Mackenzie, A., McKenzie, D., 1983. Isomerization and aromatization of hydrocarbons in sedimentary basins formed by extension. Geological Magazine 120(5), 417–470.

Makhous, M., Galushkin, Y., 2004. Basin analysis and modeling of the burial, thermal and maturation histories in sedimentary basins. Editions OPHRYS, 360 pp.

Martini, E., Reichenbacher, B., 2007. Nannoplankton und fisch-otolithen in den Mittleren Pechelbronn-Schichten (Unter-Oligozän, Oberrheingraben/Mainzer Becken). Geologische Abhandlungen Hessen 116, 235–73.

Marzi, R., 1992. Qualitative and quantitative evolution and kinetics of biological marker transformations-laboratory experiments and application to the Michigan Basin. In: Moldowan, J.M., Albrecht, P., Philp, R.P. (eds) Biological markers in sediments and petroleum. Prentice-Hall, Englewood Cliffs, NJ, 18–41.

Mazurek, M., Hurford, A.J., Leu, W., 2006. Unravelling the multi-stage burial history of the Swiss Molasse Basin: integration of apatite fission track, vitrinite reflectance and biomarker isomerisation analysis. Basin Research 18(1), 27–50.

Megnien, C., 1980. Tectogenese du Bassin de Paris; etapes de l'evolution du bassin. Bulletin de la Société géologique de France 7(4), 669–680.

Ménillet, F., Durand, M., Genter, A., Party, J., 2015. Notice explicative de la carte géologique de France (1/50 000). Feuille Haguenau (198)(2e éd.). BRGM, Orléans.

Ménillet, F., Vogt, H., Reichelt, R., Schumacher, E., Van Werveke, L., Haug, E., Bucking, H., Gross, J., Schirardin, J., Thévenin, A., 1979. Carte géologique France (1/50 000), feuille Bouxwiller (197) Orléans: BRGM 59.

Meyer, R., 1976. Continental sedimentation, soil genesis and marine transgression in the basal beds of the Cretaceous in the east of the Paris Basin. Sedimentology 23(2), 235–253.

Moldowan, J.M., Sundararaman, P., Schoell, M., 1986. Sensitivity of biomarker properties to depositional environment and/or source input in the Lower Toarcian of SW-Germany. Organic Geochemistry 10(4-6), 915–926.

Peters, K.E., 1986. Guidelines for evaluating petroleum source rock using programmed pyrolysis. AAPG bulletin 70(3), 318–329.

Philippi, G., 1965. On the depth, time and mechanism of petroleum generation. Geochimica et Cosmochimica Acta 29(9), 1021–1049.

Poelchau, H., Baker, D., Hantschel, T., Horsfield, B., Wygrala, B., 1997. Basin simulation and the design of the conceptual basin model, in: Petroleum and Basin Evolution. Springer, 3–70.

Robert, P., 1985. Histoire géothermique et diagenèse organique. Bulletin des Centres de Recherches Exploration-Production ELF-Aquitaine, Pau, Mém. 8, 345 pp.

Robin, C., 1995. Mesure stratigraphique de la déformation: application à l'évolution Jurassique du Bassin de Paris: Application à l'évolution jurassique du Bassin de Paris. Doctoral Dissertation, Université de Rennes 1, Mém. Géosciences-Rennes 77, 293 pp.

Röhl, H.-J., Schmid-Röhl, A., Oschmann, W., Frimmel, A., Schwark, L., 2001. The Posidonia Shale (Lower Toarcian) of SW-Germany: an oxygen-depleted ecosystem controlled by sea level and palaeoclimate. Palaeogeography, Palaeoclimatology, Palaeoecology 165(1-2), 27–52.

Ronov, A., 1958. Organic carbon in sedimentary rocks (in relation to the presence of petroleum). Geochemistry 5, 497–509.

Roussé, S., 2006. Architecture et dynamique des séries marines et continentales de l'oligocène moyen et supérieur du sud du fossé rhénan : Evolution des milieux de dépôt en contexte de rift en marge de l'avant-pays alpin. Doctoral Dissertation, Université de Strasbourg, 474 pp.

Ruffell, A., 1991. Sea-level events during the Early Cretaceous in Western Europe. Cretaceous Research 12(5), 527–551.

Rullkötter, J., Marzi, R., 1988. Natural and artificial maturation of biological markers in a Toarcian shale from northern Germany. Organic Geochemistry 13(4-6), 639–645.

Sanjuan, B., Gourcerol, B., Millot, R., Rettenmaier, D., Jeandel, E., Rombaut, A., 2022. Lithium-rich geothermal brines in Europe: An up-date about geochemical characteristics and implications for potential Li resources. Geothermics 101, 102385.

Scheck-Wenderoth, M., Krzywiec, P., Zühlke, R., Maystrenko, Y., Froitzheim, N., 2008. Permian to Cretaceous tectonics. In: The Geology of Central Europe, Volume 2: Mesozoic and Cenozoic. The Geological Society Publishing House, London, pp. 999–1030.

Schirardin, J., 1960. Sur la limite du Toarcien et de l'Aalénien en Alsace. Sciences Géologiques, bulletins et mémoires 13(3), 95–126.

Schmoker, J.W., Gautier, D.L., 1988. Sandstone porosity as a function of thermal maturity. Geology 16(11), 1007–1010.

Schmoker, J.W., Hester, T.C., 1989. Regional trends of sandstone porosity versus vitrinite reflectance—a preliminary framework. Presented at the AAPG Rocky Mountain Section meeting, AAPG Bulletin, Albuquerque, NM (USA) 73(CONF-8910195-).

Schnaebele, R., 1948. Monographie géologique du champ pétrolifère de Pechelbronn. Mém. Serv. Carte géol. Als. Lorr. 7, 254 pp.

Schuler, M., 1990. Environnements et paléoclimats paléogènes. Palynologie et biostratigraphie de l'Eocène et de l'Oligocène inférieur dans les fossés rhénan, rhodanien et de Hesse. Documents B.R.G.M. (190), 503 pp.

Schumacher, M.E., 2002. Upper Rhine Graben: Role of preexisting structures during rift evolution. Tectonics 21(1), 6–1.

Schwarz, F., 2021. Le pays de Pechelbronn. Un territoire façonné par l'industrie pétrolière. Revue d'Alsace, (147), 239–268.

Seifert, W., Moldowan, J., 1986. Use of biological markers in petroleum exploration. Methods in geochemistry and geophysics 24, 261–290.

Seifert, W.K., Moldowan, J.M., 1980. The effect of thermal stress on source-rock quality as measured by hopane stereochemistry. Physics and Chemistry of the Earth 12, 229–237.

Sissingh, W., 1998. Comparative tertiary stratigraphy of the Rhine Graben, Bresse Graben and Molasse Basin: correlation of Alpine foreland events. Tectonophysics 300(1-4), 249–284.

Sissingh, W., 2006. Syn-kinematic palaeogeographic evolution of the West European Platform: correlation with Alpine plate collision and foreland deformation. Netherlands Journal of Geosciences 85(2), 131–180.

Sittler, C., 1965. Le Paléogène des fossés rhénan et rhodanien. Etudes sédimentologiques et paléoclimatiques, Mém. Serv. Carte Géol. Alsace Lorraine, (24), 329 pp.

Sittler, C., 1967. Le soubassement et le remplissage sédimentaire du Fossé Rhénan au niveau du Bassin de Pechelbronn et du Seuil d'Erstein. Coupes géologiques à travers le fossé rhénan. Abh. Geol. Landesamt Baden-Württemberg, 6, Freiburg et Publ. Serv. Carte géol. Als. Lorr., Strasbourg (The Rhinegraben Progress Report 1967), 69-80.

Sittler, C., Ollivier-Pierre, M.-F., 1994. Palynology and palynofacies analyses: some essential clues to assess and identify West-European Tertiary depositional environments in terms of relative high or lowstands. Application to the case of three Eocene and Oligocene sections in France. Bulletin des centres de recherches exploration-Production Elf-Aquitaine 18(2), 475–488.

Stahmer, G., 1980. Stratigraphie des Oberrheingraben-Tertiärs und seiner nördlichen Fortsetzungen. (Interner Bericht). Wintershall AG, Kassel.

Sugden, M.A., Abbott, G.D., 2002. The stereochemistry of bound and extractable pentacyclic triterpenoids during closed system pyrolysis. Organic geochemistry 33(12), 1515–1521.

Thomas, R., Schulz, R., 2007. Facies differentiation of the Malm by interpretation of reflection seismic profiles and a moving source VSP experiment. Presented at the Proceedings European Geothermal Congress 2007, Unterhaching, Germany.

Timar-Geng, Z., Fügenschuh, B., Wetzel, A., Dresmann, H., 2006. Low-temperature thermochronology of the flanks of the southern Upper Rhine Graben. International Journal of Earth Sciences 95(4), 685–702.

Tissot, B., Durand, B., Espitalie, J., Combaz, A., 1974. Influence of nature and diagenesis of organic matter in formation of petroleum. AAPG Bulletin 58(3), 499–506.

Walter, R., 1995. Geologie von mitteleuropa. Schweizerbart, Stuttgart, Germany, 566 pp.

Wannesson, J., 1998. Alsace-Rapport régional d'évaluation pétrolière. Institut Français du pétrole, Technical report, (96), 62 pp.

Waples, D.W., Kamata, H., Suizu, M., 1992a. The art of maturity modeling, part 1: finding a satisfactory geologic model. AAPG bulletin 76(1), 31–46.

Waples, D.W., Suizu, M., Kamata, H., 1992b. The art of maturity modeling. Part 2: Alternative models and sensitivity analysis. AAPG bulletin 76(1), 47–66.

Welte, D.H., 1966. Kohlenwasserstoffgenese in Sedimentgesteinen: Untersuchungen über den thermischen Abbau von Kerogen unter besonderer Berücksichtigung der n-Paraffinbildung. Geologische Rundschau 55(1), 131–144.

Wetzel, A., Allenbach, R., Allia, V., 2003. Reactivated basement structures affecting the sedimentary facies in a tectonically "quiescent" epicontinental basin: an example from NW Switzerland. Sedimentary Geology 157(1-2), 153–172.

Yalcin, M., Littke, R., Sachsenhofer, R., 1997. Thermal history of sedimentary basins. In: Petroleum and Basin Evolution. Springer, 71–167.

Yang, S., Horsfield, B., 2020. Critical review of the uncertainty of Tmax in revealing the thermal maturity of organic matter in sedimentary rocks. International Journal of Coal Geology 225, 103500.

Ziegler, P.A., 1987. Late Cretaceous and Cenozoic intra-plate compressional deformations in the Alpine foreland—a geodynamic model. Tectonophysics 137(1-4), 389–420.

Ziegler, P.A., 1990. Geological atlas of western and central Europe. Shell Int. Pet. Maatschappij, Geol. Soc. Publ. House, Bath, UK, 239 pp.

Ziegler, P.A., 1994. Cenozoic rift system of Western and Central-Europe: An overview. Geologie en Mijnbouw 73(2-4), 99–127.

Ziegler, P.A., Dèzes, P., 2005. Evolution of the lithosphere in the area of the Rhine Rift System. International Journal of Earth Sciences 94(4), 594–614.

Zumberge, J.E., 1987. Terpenoid biomarker distributions in low maturity crude oils. Organic geochemistry 11(6), 479–496.